

Modeling the Dynamic Interaction of Hebbian and Homeostatic Plasticity

Taro Toyozumi,^{1,2,3,*} Megumi Kaneko,⁴ Michael P. Stryker,⁴ and Kenneth D. Miller^{2,5}

¹RIKEN Brain Science Institute, 2-1 Hirosawa, Wako, Saitama 351-0198, Japan

²Center for Theoretical Neuroscience and Department of Neuroscience, College of Physicians and Surgeons, Columbia University, 1051 Riverside Drive, New York, NY 10032, USA

³Department of Computational Intelligence and Systems Science, Tokyo Institute of Technology, Yokohama 226-8502, Japan

⁴Center for Integrative Neuroscience and Department of Physiology, University of California, 675 Nelson Rising Lane, San Francisco, San Francisco, CA 94158, USA

⁵Kavli Institute for Brain Science, Columbia University, 1051 Riverside Drive, New York, NY 10032, USA

*Correspondence: taro.toyoizumi@brain.riken.jp

<http://dx.doi.org/10.1016/j.neuron.2014.09.036>

SUMMARY

Hebbian and homeostatic plasticity together refine neural circuitry, but their interactions are unclear. In most existing models, each form of plasticity directly modifies synaptic strength. Equilibrium is reached when the two are inducing equal and opposite changes. We show that such models cannot reproduce ocular dominance plasticity (ODP) because negative feedback from the slow homeostatic plasticity observed in ODP cannot stabilize the positive feedback of fast Hebbian plasticity. We propose a model in which synaptic strength is the product of a synapse-specific Hebbian factor and a postsynaptic-cell-specific homeostatic factor, with each factor separately arriving at a stable inactive state. This model captures ODP dynamics and has plausible biophysical substrates. We confirm model predictions experimentally that plasticity is inactive at stable states and that synaptic strength overshoots during recovery from visual deprivation. These results highlight the importance of multiple regulatory pathways for interactions of plasticity mechanisms operating over separate timescales.

INTRODUCTION

Hebbian plasticity and homeostatic plasticity are the two major forms of activity-dependent plasticity that modify neuronal circuits (Turrigiano, 2008). We use “Hebbian plasticity” to refer to plasticity that depends on the correlations between pre- and postsynaptic activity such that excitatory synapses that effectively drive a postsynaptic cell grow stronger while ineffective synapses are weakened. This is a positive feedback process—strong synapses grow stronger—that in models typically leads to synaptic instability in the absence of additional biological constraints (Miller and MacKay, 1994; Turrigiano, 2008). Synaptic homeostasis is a negative feedback mechanism that typically

involves nonspecific scaling of all excitatory or inhibitory synapses onto a cell to oppose changes in overall activity levels. This is thought to maintain activity levels within a dynamic range and, more generally, to stabilize neuronal circuit function despite the positive feedback of Hebbian plasticity (Turrigiano, 2008). It is not known how these two forms of plasticity interact in biological systems (Shepherd and Huganir, 2007; Turrigiano, 2011, 2008).

Ocular dominance plasticity (ODP) in primary visual cortex (V1) has been a standard system in which to study experience-dependent plasticity (Espinosa and Stryker, 2012). During the critical period for ODP, monocular deprivation (MD)—the closure of one eye—induces rapid weakening of responses to the closed eye and subsequent strengthening of responses to the open eye (Frenkel and Bear, 2004; Hofer et al., 2006; Mrsic-Flogel et al., 2007). A recovery period with binocular vision following MD causes both eyes' response levels to return to normal. Recently, three separable processes have been identified underlying this plasticity in mouse V1 (Kaneko et al., 2008a, 2008b):

- (1) Weakening of the closed eye's responses is rapid, occurring over the first 3 days of MD, and appears to be mediated by Hebbian plasticity because of its dependence on calcium entry through N-methyl-D-aspartate (NMDA) receptors acting on calcium calmodulin kinase type II (Taha et al., 2002). This weakening shares other molecular features of Hebbian long-term depression (LTD) (Heynen et al., 2003; Yoon et al., 2009) but differs from LTD in its dependence on protein synthesis (Lee et al., 2003; Shepherd and Huganir, 2007; Taha and Stryker, 2002). It is not affected by blockade of tumor necrosis factor- α (TNF- α) or the tropomyosin-related kinase B (TrkB) receptor (Kaneko et al., 2008a, 2008b).
- (2) Strengthening of the open eye is slower, commencing only after about 3 days, and appears to be mediated by homeostatic synaptic scaling; it is specifically prevented by blockade of TNF- α (but not of TrkB) (Kaneko et al., 2008a, 2008b), which induces a global form of homeostatic synaptic scaling (Stellwagen and Malenka, 2006). TNF- α induces a uniform scaling up of the strengths of excitatory synapses in response to a lowering of overall

activity levels. This occurs without alteration in Hebbian plasticity as assessed by the percentage changes of synaptic strengths induced by long-term potentiation (LTP) or LTD (Stellwagen and Malenka, 2006).

- (3) Recovery from MD under binocular vision is specifically prevented by blockade of TrkB (Kaneko et al., 2008a). TrkB has a variety of actions on synaptic plasticity. It is required for the growth of new synapses in neuronal cell culture (Meyer-Franke et al., 1998) and is involved in stabilization of Hebbian LTP (Figurov et al., 1996; Kovalchuk et al., 2002; Lai et al., 2012; Sermasi et al., 2000; Tanaka et al., 2008).

The slow onset of homeostatic scaling, relative to the fast onset of Hebbian plasticity, poses a problem. Synaptic dynamics under Hebbian plasticity alone are typically unstable until synaptic strengths (“weights”) are driven to saturation near maximum or minimum allowed values (e.g., Miller and MacKay, 1994). In models that combine Hebbian with homeostatic plasticity (or with mechanisms similar to homeostatic plasticity, such as multiplicative normalization of synaptic strengths or metaplasticity), homeostatic plasticity generally stabilizes a set of unsaturated weights that would be unstable under Hebbian plasticity alone (von der Malsburg, 1973; Bienenstock et al., 1982; Oja, 1982; Cooper et al., 2004; Miller and MacKay, 1994; Toyozumi and Miller, 2009; Toyozumi et al., 2013). However, such stabilization fails if homeostatic plasticity is too slow compared to unstable Hebbian plasticity (Cooper et al., 2004; Zenke et al., 2013). This is an example of the more general result that slow negative feedback cannot stabilize a fast, unstable positive feedback process. Thus, the slow onset suggests that homeostasis cannot stabilize Hebbian ODP.

To solve this problem, Hebbian plasticity must arrive on its own at a stable steady state, and this stability must not be disturbed by slow, ongoing homeostatic plasticity. We show that this solution can be instantiated and the experimental results robustly reproduced by a simple model in which the total synaptic strength is the product of two factors: a synapse-nonspecific factor, applicable to the entire postsynaptic cell, controlled by homeostatic plasticity and a synapse-specific factor controlled by Hebbian plasticity. In addition to demonstrating the model’s ability to account for existing results, we test several key predictions of the model experimentally, including a lack of constitutive but opposed Hebbian and homeostatic plasticity at a stable state of the weights and a TNF- α -dependent overshoot of formerly closed-eye weights upon reopening of the closed eye after MD.

RESULTS

MD Effects on Single-Synapse Plasticity Models in the Monocular Cortex

In monocular cortex, which receives input only from the contralateral eye, similar dynamics of Hebbian and homeostatic plasticity are seen as in binocular cortex. During the first 3 days of MD, the strength of the closed eye’s input decreases by about 25%–30% in an NMDA receptor-dependent manner (Frenkel and Bear, 2004; Heynen et al., 2003; Kaneko et al., 2008a). Dur-

ing the subsequent 3 days of MD, the closed-eye input strength homeostatically increases back to near-baseline levels, an increase dependent on TNF- α (Kaneko et al., 2008b). Although this dynamical behavior under MD is simple, existing models cannot reproduce it, as we will show, because homeostatic plasticity that is slow enough to allow significant initial depression of the synaptic weight is too slow to stabilize plasticity.

We consider in this section a very simple, one-synapse model of monocular cortex: a single postsynaptic cell with activity y receives a single input with synaptic strength w and activity x . We assume the output activity is given by $y = wx$ and take the input activity x to be constant in each condition, $x = 1$ for normal visual experience, and $x < 1$ under MD (for simplicity we take activities and weights to be unitless numbers). By assuming a single input, we are in essence assuming that the synapses projecting to the monocular cortex are relatively homogeneous so that w and x indicate the average synaptic strength from and average activity of the LGN inputs from the contralateral eye. Similarly, y indicates the average activity of monocular cortex. Later in the paper we consider a heterogeneous population of inputs in binocular cortex and show that the conclusions reached here are unchanged.

The BCM Rule

A learning rule that is commonly used to describe ODP and that includes both Hebbian and homeostatic elements is the Bienenstock-Cooper-Munro (BCM) rule (Bienenstock et al., 1982; Cooper et al., 2004). In this model, an active input ($x > 0$) undergoes LTP if the postsynaptic activity y is greater than a threshold θ and undergoes LTD if $y < \theta$; this is the Hebbian element. With the simple system considered here, this part of the BCM rule can be written as

$$\tau_w \frac{dw}{dt} = xy(y - \theta), \quad (\text{Equation 1})$$

where τ_w is a time constant that sets the Hebbian learning rate.

The homeostatic element of the BCM rule arises through the dynamic adjustment of θ over time to keep average postsynaptic activity near a set-point activity level, y_0 . θ is a superlinear function of the average firing rate, typically $\theta = \bar{y}^2 / y_0$, where \bar{y}^2 is the average of y^2 over some averaging time. Taking this averaging time to be τ_θ , the dynamics of θ can be written as follows:

$$\tau_\theta \frac{d\theta}{dt} = -\theta + y \frac{y}{y_0}. \quad (\text{Equation 2})$$

When the model is switched to the MD condition, the weight initially decreases and subsequently increases. Consider starting at the fixed point for the normal ($x = 1$) condition, $y = \theta = w = y_0$. Immediately after MD onset, input activity x , and thus $y = wx$, is reduced, so $y < \theta$. This causes LTD under Equation 1 and, thus, further reduction in y . However, since $y < y_0$, θ moves toward an equilibrium value $y(y/y_0)$ that is less than y . Once θ becomes less than y , the Hebbian rule causes LTP and y rises.

The speed of the decrease in θ , and thus of the switch from LTD to LTP, is determined by the time constant τ_θ (Equation 2). The speed of LTD is controlled by τ_w (Equation 1). In order to have significant initial LTD, τ_θ must be sufficiently large, relative

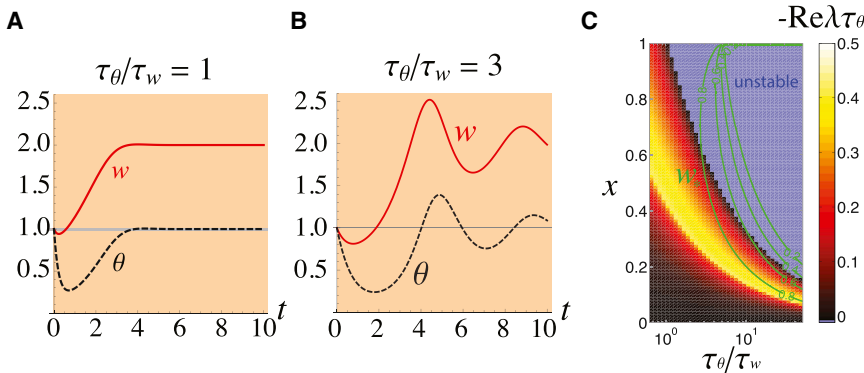


Figure 1. The Dynamics of the Synaptic Strength under the BCM Learning Rule in the Monocular Cortex during MD Initiated at Time 0

(A–C) The synaptic strength w (red line) and the activity-dependent threshold θ (black dashed line) were plotted versus time for homeostatic plasticity that is the same speed as (A: $\tau_\theta = \tau_w$) or slower than (B: $\tau_\theta = 3\tau_w$) Hebbian plasticity. The initial condition ($t = 0$) was set to the fixed point under normal rearing (which is unstable for $\tau_\theta = 3\tau_w$, see C). For faster homeostatic plasticity, there is little initial depression of synaptic strength (A). When the homeostasis is slowed, however, the normal-rearing fixed point becomes unstable (c.f. C), and the synaptic strength exhibits large oscillations under

MD (B). We took the set-point activity to be $y_0 = 1$, which sets the units of activity. We set input activity $x = 1$ in the normal condition, $x = 1/2$ under MD. We set $\tau_w = 0.2$ days; numbers on the x axis represent days. (C) A systematic study of the BCM learning rule, as a function of input activity x and speed of homeostatic plasticity, τ_θ/τ_w . We characterized the dynamics of synaptic strength under MD by two variables: the depth of synaptic depression, measured as the strength w_s at the first trough of synaptic strength relative to the pre-MD ($x = 1$) strength of $w = 1$ (green contour lines); and the stability of the fixed point $w = 1/x$, as measured by the stability index $-\text{Re}\lambda\tau_\theta$ (color plot; more positive values of the stability index indicate greater distances from instability; negative values mean the fixed point is unstable). Here, λ is the eigenvalue with greatest real part of the system linearized about the fixed point. For choices of x and τ_θ/τ_w that reproduce $w_s \sim 0.7$, as in experiments, the synaptic strength dynamics are unstable for a wide range of x including the normal rearing condition $x = 1$. The results shown in this figure are general and do not depend on any specific parameter choices (e.g., choosing $x = 1$ to represent normal rearing), as explained in [Supplemental Information Section S1](#).

to τ_w , so that significant LTD occurs before θ adapts. When τ_θ/τ_w is sufficiently small, θ adapts quickly, before the synaptic weight significantly changes, so that there is very little initial synaptic depression (Figure 1A). However, as τ_θ/τ_w is increased, the fixed point under normal rearing becomes unstable even as the degree of synaptic depression under MD (initiated with this unstable normal-rearing fixed point as initial condition) remains small (Figure 1C; see also [Supplemental Information Section S1](#), available online), and this MD leads to large oscillations of synaptic strengths (Figure 1B). The oscillations arise because when y reaches y_0 , θ still reflects the earlier weight values, so weight change continues in the same direction until θ catches up. Instability occurs when the threshold change is so slow that the threshold never catches up (Cooper et al., 2004; Zenke et al., 2013) (when $\tau_\theta/\tau_w > 1/(x^2 y_0)$ for Equations 1 and 2).

In the BCM model, both dw/dt and $d\theta/dt$ are zero at the fixed point. However, biological weights will constantly fluctuate under ongoing changes in activity. Such fluctuations induce destabilizing Hebbian plasticity, which can only be stabilized by fast homeostatic plasticity (i.e., fast changes in θ). In this sense, the BCM model requires that the two forms of plasticity are constitutively active but opposed in the vicinity of any fixed point.

Addition of Stable Hebbian Terms and a Homeostatic Term

To try to prevent loss of stability with slow homeostatic plasticity, we next consider an intrinsically stable Hebbian rule. In addition, we would like the model to be physiologically realistic in three respects in which the BCM rule is not. First, LTP and LTD should saturate, whereas in the BCM rule there is no limit to synaptic potentiation and LTD can reduce weights to zero. Second, in a model with multiple synapses, homeostatic plasticity should multiplicatively scale synaptic strengths, preserving the relative strengths of different synapses, as suggested by homeostatic

scaling of the distribution of miniature excitatory postsynaptic potentials (mEPSPs) (Turrigiano et al., 1998; Stellwagen and Malenka, 2006; Kaneko et al., 2008b; Turrigiano, 2011). The sliding threshold of the BCM rule does not produce multiplicative changes in synaptic strengths. Third, homeostatic plasticity occurs under blockade of activity through bath application of tetrodotoxin (TTX) or under blockade of NMDA receptors, both in vitro (TTX, Turrigiano et al., 1998; NMDA block, Kaneko et al., 2008b; both, Stellwagen and Malenka, 2006) and in vivo in V1 during the critical period (TTX, Maffei and Turrigiano, 2008; NMDA, see Figure 7A). Under the BCM rule there is no plasticity when the pre- or the postsynaptic firing rate is zero or when NMDA receptors are blocked.

We again consider our one-input model of the monocular cortex. We assume that synaptic strength is modified by the sum of an LTP term, an LTD term, and a multiplicative homeostatic term. LTP occurs when the product of pre- and postsynaptic activities, xy , is greater than a fixed threshold θ , while LTD occurs for $xy < \theta$. To make the Hebbian plasticity intrinsically stable, the LTP and LTD terms saturate when the weight w reaches a maximal value w_{\max} or minimal value w_{\min} , respectively, consistent with experiments suggesting a limited range of strengths of individual synapses (O'Connor et al., 2005; Petersen et al., 1998). A nonzero minimal weight value is important because multiplicative homeostatic plasticity cannot potentiate synaptic strength if it reaches zero. The homeostatic term changes the weight to move the time-averaged postsynaptic activity \bar{y} toward the set-point value y_0 . This term induces weight change proportional to w , which—once we consider multiple inputs—will make the homeostasis multiplicative, scaling all weights by a common factor rather than adding or subtracting a common amount from all weights. A parameter γ determines the strength (or, equivalently, the learning speed) of homeostasis relative to Hebbian plasticity.

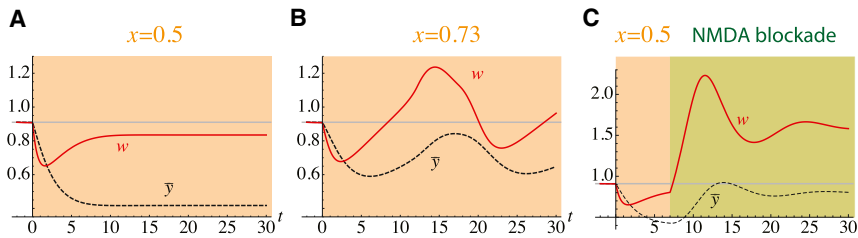


Figure 2. Simulation Results of Plasticity in the Monocular Cortex during MD, Using a Learning Rule with a Stable Hebbian Component and a Homeostatic Component (Equations 3 and 4).

(A–C) The synaptic strength, w , and the average postsynaptic activity, \bar{y} , are plotted for stronger MD (A; $x = 0.5$) and weaker MD (B; $x = 0.73$). For the model to reproduce the experimental result, as in (A), parameters must be tuned so that the dynamics remain relatively near the stable fixed point under Hebbian plasticity alone.

When the combined Hebbian/homeostatic dynamics move sufficiently far from that fixed point, the Hebbian dynamics are unstable and cannot be stabilized by slow homeostatic plasticity, yielding oscillations (B) or instability. The MD fixed point in (A), though nonoscillatory, involves constitutive but opposed LTD and homeostatic plasticity so that blockade of Hebbian plasticity beginning at day 7 of MD yields a marked homeostatic increase in weight (C). Parameters: $w_{\max} = 1$, $w_{\min} = 0.6$, $\tau_w = 0.3$ day, $\tau_{\bar{y}} = 3$ days, $y_0 = 0.8$, $\theta = 0.6$, $\gamma = 0.23$. x axis: time in days.

We let $[x]_+$ represent the operation of setting negative values to zero, that is, $[x]_+ = x$ when $x > 0$, and $[x]_+ = 0$ otherwise. Then the equation for weight change is

$$\tau_w \frac{dw}{dt} = [w_{\max} - w]_+ [xy - \theta]_+ - [w - w_{\min}]_+ [\theta - xy]_+ + \gamma w (1 - \bar{y}/y_0). \quad (\text{Equation 3})$$

The first term in Equation 3 is the LTP term, the second is the LTD term, and the third is the homeostatic term. This equation does not have the problems just noted for the BCM rule: in Equation 3, LTP and LTD both saturate, homeostatic plasticity induces a multiplicative scaling of weights, and homeostatic plasticity will occur even in the absence of pre- or postsynaptic activity.

The delay in the signal driving homeostatic learning is determined by the time, $\tau_{\bar{y}}$, over which the postsynaptic activity is averaged to produce \bar{y} . Assuming an exponentially weighted average with time constant $\tau_{\bar{y}}$, the equation for \bar{y} is

$$\tau_{\bar{y}} \frac{d\bar{y}}{dt} = -\bar{y} + y. \quad (\text{Equation 4})$$

We choose parameters to reproduce the results of MD in the monocular cortex (Kaneko et al., 2008b) (see Supplemental Information Section S2). This model can reproduce fast LTD and slow homeostatic plasticity in the monocular cortex under MD. However, this outcome was fragile and sensitive to parameter values. Figure 2A shows the simulated result of the plasticity rule under strong MD ($x = 0.5$). The synaptic weight rapidly decreased and reached about 70% of the pre-MD value after 2 days of MD. Delayed homeostatic plasticity then started, due to the loss of postsynaptic activity, and scaled up the synaptic strength to about 90% of the pre-MD value. This result is consistent with the experimental observation. However, the result depended sensitively on the input strength under MD. Figure 2B shows a result of a simulation under weaker MD ($x = 0.73$). In this case, the synaptic strength settled into a stable oscillation (see phase plane analysis, Supplemental Information Section S3, and Figure S1).

This behavior is similar to that of the BCM rule explored previously. The problem is a general one that does not depend on arbitrary details of the implementation (e.g., use of a threshold nonlinearity $[x]_+$ as opposed to more smooth nonlinearities); for sufficiently slow homeostatic plasticity, there will be input values yielding oscillations or instability. The saturation limits

ensure that the Hebbian terms in Equation 3, by themselves, have a stable fixed point. However, the system's fixed point—the steady-state values of w and \bar{y} of the entire system, including the homeostatic term—may be at values of w distinct from this Hebbian-only fixed point. When the two fixed points are sufficiently far apart, small perturbations of w away from the fixed point will be amplified by fast Hebbian positive feedback, and the slow homeostatic negative feedback through change in \bar{y} either cannot catch up (instability) or takes a long time to catch up (oscillations). In sum, system stability depends on choosing parameters for which the Hebbian and system fixed points are sufficiently near, but they are unlikely to remain near across multiple input values. We are once again faced with the fact that slow homeostatic plasticity cannot stabilize fast, unstable (positive feedback) dynamics.

Even when the MD fixed point is near enough to the Hebbian fixed point to prevent oscillations (Figure 2A), LTD and homeostatic upscaling are constitutively active but cancelling. We show in Section S2 of the Supplemental Information that such constitutive plasticity always occurs at fixed points of Equations 3 and 4 for values of x outside of a finite range. As a result, if Hebbian plasticity is blocked, a large homeostatic change in the synaptic weight will occur (Figure 2C), a possibility we now test.

Experimental Test I: Lack of Constitutive Plasticity at Steady States

As we have just seen, plasticity models in which Hebbian and homeostatic plasticity compete to directly alter a single factor, w , make the general prediction that, for at least some rearing conditions, Hebbian and system fixed points should not coincide. This means that Hebbian and homeostatic plasticity are both constitutively active at the system steady state, inducing equal and opposite weight changes that cancel. While a rule might have both forms of plasticity separately zero at one steady state, it would require fine-tuning of parameters for separate cancellations to occur at multiple steady states corresponding to different rearing conditions.

To test this prediction experimentally, we blocked Hebbian plasticity by a partial blockade of NMDA receptors using daily intraperitoneal injection of a low dose of the NMDA receptor inhibitor 3-(2-carboxypiperazin-4-yl)propyl-1-phosphonic acid (CPP). This regime was shown to block NMDA-receptor-dependent plasticity in mouse V1 (in the same strain of mice studied here) during the critical period and in adulthood; it blocks

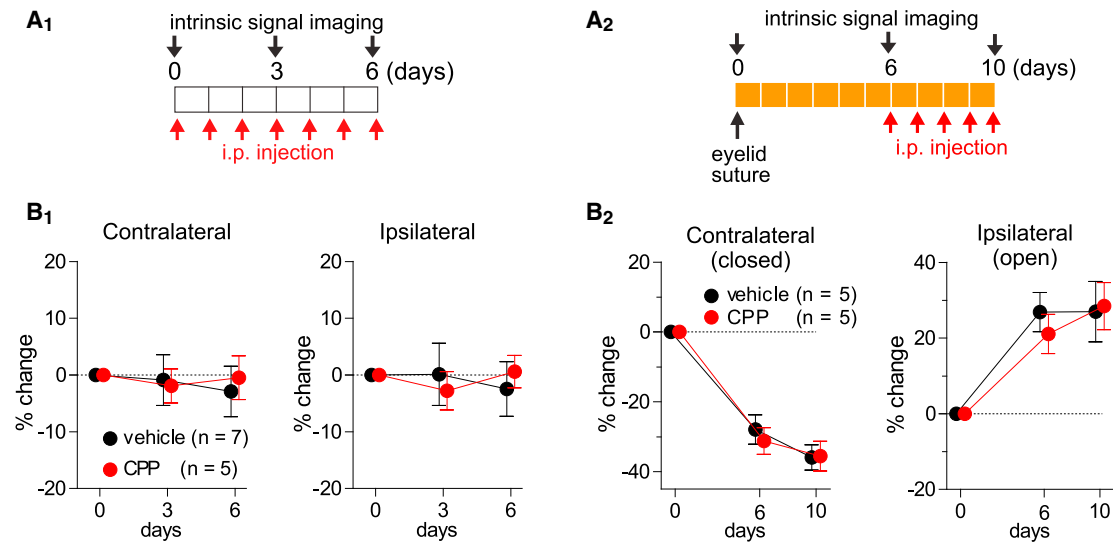


Figure 3. Lack of Constitutive Plasticity at Steady States

(A and B) Hebbian plasticity and homeostatic plasticity are each separately inactive under normal rearing (A₁ and B₁) and after 6 days of monocular deprivation (A₂ and B₂). (A) Experimental designs. An NMDA receptor antagonist (CPP) or vehicle solution was injected intraperitoneally for 6 days under normal rearing (A₁) or for the last 4 days of a 10-day MD period (A₂). (B) In each case, responses in binocular V1 to stimulation through each eye were unchanged by the NMDA receptor block, suggesting a lack of ongoing plasticity in these conditions. Baseline response levels were indistinguishable in CPP and control animals (Figure S7). Data are represented as mean \pm SEM.

NMDA-receptor-dependent expression of the immediate early gene product *Zif268* and blocks ODP in response to MD but does not block visual behavior or the responses of neurons in mouse V1 (Sato and Stryker, 2008). As we will discuss later, it leaves homeostatic plasticity intact, while appearing to block Hebbian plasticity, when applied during days 4–7 of MD (Figure 7A). We injected CPP during each of two different, approximately steady states during the critical period for ODP in mice: during normal rearing and during the last 3 days of a 10-day MD (Figure 3). At each steady state, the blockade caused no significant change in either eye's response strength in V1, as assessed with intrinsic signal imaging, relative to control animals (daily vehicle injection), in contrast to the outcome seen in Figure 2C. This indicates that Hebbian and homeostatic plasticity are each separately nearly zero at each of the two steady states.

Note that this experiment does not speak against the BCM model. In that model, all plasticity is stopped by NMDA receptor blockade. However, we have noted other empirical problems with the BCM model.

Our Proposed Solution: A Model with Hebbian and Homeostatic Factors that Multiply to Produce Synaptic Strength

We have seen that the observed combination of fast synaptic depression and slow homeostatic plasticity after MD cannot be robustly reproduced by traditional plasticity models in which the Hebbian and homeostatic components directly compete to control the same factor. Furthermore, the constitutive, equal, and opposite forms of plasticity predicted to exist at a steady state by models with separate, competing homeostatic and Hebbian terms were not found experimentally.

This motivates our proposed solution: a model in which a synapse-specific Hebbian factor, ρ , and a postsynaptic-cell-specific homeostatic factor, H , each with their own learning dynamics, are multiplied to give the synaptic strength: $w = H\rho$ (Figure 4A). LTP and LTD rapidly modify ρ in an NMDA-dependent manner, while homeostatic plasticity more slowly modifies H through the effects of $\text{TNF-}\alpha$ and perhaps other factors. This model is consistent with the experimental result that the percentage of synaptic strength changes induced by Hebbian LTP or LTD protocols were unchanged by modifications of homeostatic plasticity (pretreatment with $\text{TNF-}\alpha$ or knockout of $\text{TNF-}\alpha$ receptors; Stellwagen and Malenka, 2006).

In our proposed model, the dynamics of ρ —the Hebbian dynamics—are stable by themselves, reaching a stable fixed point for the given input statistics. We will assume this stabilization is achieved through saturation of ρ at minimal and maximal allowed values (O'Connor et al., 2005; Petersen et al., 1998), but any stable Hebbian learning rule would suffice. The homeostatic dynamics still involve slow learning, but because of the relationship $w = H\rho$, such slow dynamics will scale the weights—including the minimal and maximal weights—to bring the overall activity level toward the desired set point without disturbing the intrinsic stability of the Hebbian dynamics. In this model, the synaptic strength does not oscillate because homeostatic plasticity is driven by the instantaneous activity without the delays of slow time averaging. In the previous models, the observed slowness of homeostatic plasticity had to arise from slow time averaging rather than slow learning because slow learning, which means small changes per unit time, would have made the homeostatic term too weak to affect learning. That is, under slow learning, the small changes in w

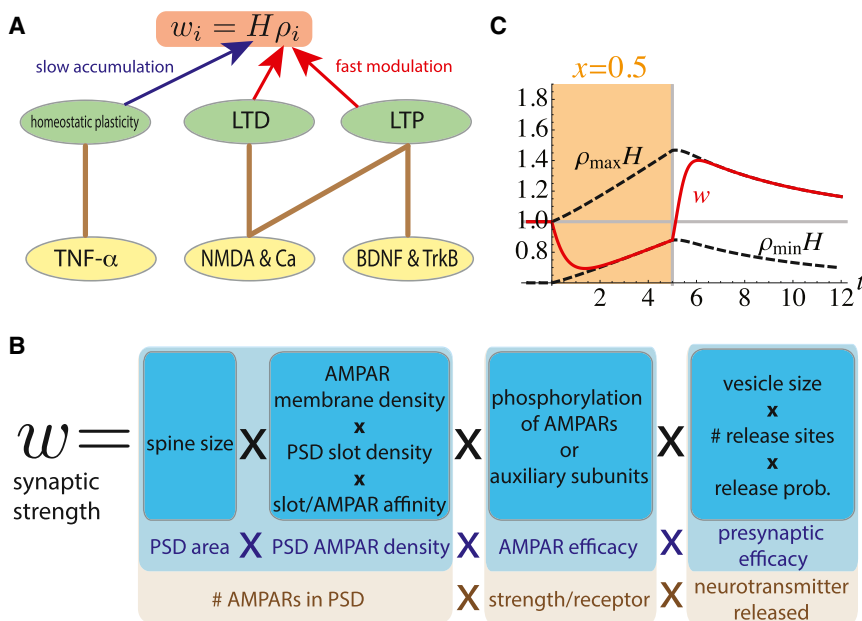


Figure 4. A Schematic Description of the Two-Factor Model

(A) The i^{th} synaptic strength is described by $w_i = H\rho_i$, where H is a synapse nonspecific homeostatic variable and ρ_i is a synapse-specific Hebbian variable. Hebbian plasticity rapidly changes ρ_i , while homeostatic plasticity slowly changes H . The slow change in H can build up without being overwritten by the fast Hebbian effect. In models in which Hebbian plasticity and homeostatic plasticity both directly change synaptic strengths, homeostatic plasticity cannot be slow without being overwritten. In the model, both LTP and LTD are mediated by NMDA-dependent calcium influx. In addition, BDNF/TrkB signaling is assumed to be required for LTP, and homeostatic plasticity is mediated by TNF- α .

(B) A biophysical interpretation of separable factors whose product is the synaptic strength: four overall factors (light blue) and corresponding biophysical elements controlling them (dark blue), including further breakup of some factors into a product of subfactors. Our model could be instantiated if H and ρ each control separate subsets of these factors or subfactors.

(C) Simulation results of the two-factor model in the monocular cortex during MD and recovery from MD. Colored regions of plots (days 0–5) represent periods of MD; white region (days 5–12) represents normal vision ($x = 1$). The plot illustrates the synaptic strength w (red line) and the maximal and minimal possible synaptic strengths, $H\rho_{\text{min}}$ and $H\rho_{\text{max}}$, which we term the limiting strengths, both represented by dashed lines. Changes in these limiting strengths represent homeostatic plasticity, i.e., changes in the homeostatic factor H . When the weight w reaches a limiting strength, it indicates the Hebbian factor ρ has reached its corresponding limiting value, ρ_{max} or ρ_{min} . The synaptic strength was rapidly depressed to the minimum value via the Hebbian component, and then this minimum value was slowly potentiated by the homeostatic component. When the eye was reopened ($x = 1$) after 5 days of MD, the synaptic strength rapidly potentiated to the maximum value by LTP, and then this maximum value was slowly depressed by the homeostatic component. x axis: time in days. Parameters used: $\theta = 0.6$, $\gamma_0 = 1$, $\rho_{\text{max}} = 1$, $\rho_{\text{min}} = 0.6$, $\tau_{\rho} = 0.2$ days, and $\tau_H = 8.0$ days.

induced by homeostasis in any given time interval would have been easily reversed by the larger changes induced by the faster Hebbian plasticity.

This two-factor model is no doubt still a simplification—an effective model—of the complex dynamics of synaptic learning (e.g., Hugarir and Nicoll, 2013), and determining the biophysical basis of this model awaits further experimental work. However, we suggest the following overall framework for interpreting the model (Figure 4B). The postsynaptic density (PSD) is thought to have a certain number of “slots” for alpha-amino-3-hydroxy-5-methyl-4-isoxazole propionic acid receptors (AMPA). These slots are created by PSD structural proteins (Hugarir and Nicoll, 2013; Kessels and Malinow, 2009), some of which play roles in homeostatic plasticity (Shin et al., 2012; Steinmetz and Turrigiano, 2010; Sun and Turrigiano, 2011). The synaptic strength, to the extent that it is determined by AMPARs, could be understood as the product of four elements: (1) the area of the PSD (which is increased by Hebbian LTP, which increases spine size: Matsuzaki et al., 2004; Harvey and Svoboda, 2007; Zhou et al., 2004; Kopec et al., 2007), (2) the density of AMPARs bound to slots in the PSD, (3) the efficacy of the AMPARs, and (4) the presynaptic efficacy, which also undergoes activity-dependent modification (Atwood and Karunanithi, 2002; Kaneko et al., 2010). If free AMPARs in the membrane and slots bind with first-order kinetics, then the PSD density of bound AMPARs can be further broken down as the product of (2a) membrane AMPAR density, known to be increased by TNF- α (Beattie

et al., 2002; Leonoudakis et al., 2008; Stellwagen and Malenka, 2006), (2b) PSD slot density, and (2c) slot/AMPA binding affinity. The latter two factors and AMPAR efficacy are likely altered by modulations (e.g., phosphorylation) and/or changes in composition of both AMPARs and PSD structural proteins. The presynaptic efficacy likewise breaks down to a product of subfactors. In sum, if the homeostatic factor H and Hebbian factor ρ each correspond to different subsets of these biophysical factors, then the product ρH would correspond to the synaptic strength.

Such a division of mechanisms fits well with the three working models proposed by Hugarir and Nicoll (2013) for how calcium-calmodulin kinase type II (CaMKII) activation causes Hebbian LTP. In their “PSD-centric” model, CaMKII alters PSD structural proteins to increase the number of slots at the given synapse (mechanism 2b). In their “receptor-centric” model, CaMKII phosphorylates AMPAR complexes to increase their binding affinity to the slots (mechanism 2c). In their “insertion” model, CaMKII drives exocytosis of vesicles containing glutamate receptors, increasing the density of AMPARs in the plasma membrane (mechanism 2a). Under any of these models, Hebbian plasticity might also control additional mechanisms and homeostasis would control one or more complementary mechanisms.

To study our proposed two-factor model, we continue to consider the framework of Figure 2A, a single presynaptic input in monocular cortex. The Hebbian factor is modeled as in the previous section so that LTP and LTD occur for $xy > \theta$ and $xy < \theta$,

respectively, and both are stabilized by saturation of ρ at maximal or minimal values:

$$\tau_{\rho} \frac{d\rho}{dt} = (\rho_{\max} - \rho)[xy - \theta]_{+} - (\rho - \rho_{\min})[\theta - xy]_{+}. \quad (\text{Equation 5})$$

The homeostatic term grows or decays if the activity is respectively below or above the desired set-point level y_0 :

$$\tau_H \frac{dH}{dt} = H \left(1 - \frac{y}{y_0} \right). \quad (\text{Equation 6})$$

The proportionality to H on the right side of Equation 6 is not important in practice but formally ensures that H remains positive. The speed of Hebbian and homeostatic learning are controlled by the time constants τ_{ρ} and τ_H , respectively. Note that H depends only on postsynaptic activity y , and not directly on the synaptic weight, so that it provides a set point for y . In a multisynapse model, this will mean that H is a postsynaptic-cell-specific, rather than synapse-specific, factor.

These equations (and also those of a multisynapse model to be studied below) can be shown to be mathematically equivalent to a model similar to that of Equation 3 in which Hebbian and homeostatic plasticity both compete to modify a single factor w , but in which homeostatic plasticity also scales the maximal and minimal allowed weights and, while slow, responds to instantaneous rather than time-averaged postsynaptic activity (Supplemental Information Section S5). The former point is critical for homeostatic plasticity to multiplicatively scale synaptic strengths without disturbing intrinsic Hebbian stability and without being overwritten by Hebbian plasticity. The latter point is critical to stability: slow averaging introduces delays that can yield oscillations of synaptic strength.

We will find that this simple model, like the previous model (Figure 2), still has behavior that varies qualitatively with the strength of MD (the value of x), although in the present case this variation might be physiologically realistic (see Supplemental Information Section S6). The key difference, however, will be that in the present model, the behavior is always stable, approaching a stable fixed point (at which each form of plasticity is separately zero) without oscillations. Further issues with the behavior can be fixed by using a more complex plasticity model, as we will see in the next section, but the stability is intrinsic to the framework of separable factors with a stable Hebbian component (Supplemental Information Section S4). In the previous model, instability was intrinsic to the framework for the reasons outlined above and could not be fixed by a more complex model.

To simulate this model, we assumed that homeostatic learning was quite slow relative to Hebbian learning to show that no instability results: τ_H was 40 times longer than τ_{ρ} (stability for any value of τ_H/τ_{ρ} is shown in Supplemental Information Section S4). Before MD, ρ was saturated at its maximal value, $\rho = \rho_{\max}$.

We simulated MD ($x = 0.5$) applied for 5 days (colored region), followed by recovery with normal vision ($x = 1$) for the next 7 days (white region; Figure 4C). Behavior of the model for MD with intermediate values of x are examined in Supplemental Information Section S6. During the 5 days of MD, the synaptic strength was first decreased through Hebbian LTD, reaching about 70% of its initial value, and then was potentiated by homeostatic

plasticity, matching experimental results well (Kaneko et al., 2008b). Restoration of normal vision at day 5 led to an overshoot of synaptic strength: a rapid increase through Hebbian LTP, followed by a slower decrease toward baseline through homeostatic plasticity. This overshoot is a robust prediction of our model given slow homeostatic and fast Hebbian plasticity: homeostatic scaling H had increased to compensate for decreased activity and Hebbian synaptic depression during MD; recovery induces a rapid LTP of ρ , yielding an overshoot of $w = \rho H$; H then slowly decreases to return the system to the set-point activity. We present below an experimental test of this prediction of an initial overshoot of synaptic strength following restoration of normal vision.

So far, we have considered the MD result only in the monocular cortex and have also neglected the heterogeneity among synapses, replacing multiple synaptic strengths by a representative value. In the next section, we consider a more realistic network model with multiple presynaptic neurons and consider binocular as well as monocular cortex.

MD Effects in Multisynapse Plasticity Models in the Binocular Cortex

We now consider multiple presynaptic neurons ($N = 500$) projecting to a postsynaptic neuron. The i^{th} input contributes an amount to the postsynaptic firing rate equal to the input's firing rate x_i times its synaptic weight w_i , and the postsynaptic firing rate is the linear sum of these contributions: $y = \sum_{i=1}^N w_i x_i$. In the binocular cortex, the postsynaptic neuron receives $N_C = 310$ synapses from the contralateral eye and $N_I = 190$ synapses from the ipsilateral eye. This ratio was chosen to reproduce the physiological ocular-dominance index (ODI) under normal rearing (Kaneko et al., 2008b). The i^{th} synaptic strength is described by $w_i = H A_i \rho_i$, where A_i is the anatomical strength of axonal arborization (Miller et al., 1989) (see Supplemental Information Section S7.2) and is normalized as $\sum_i A_i = 1$ to keep postsynaptic activity level roughly independent of the choice of N ; ρ_i is the synapse-specific Hebbian factor, and H is the synapse-nonspecific homeostatic factor characterizing the overall scaling of synaptic strengths onto the given postsynaptic neuron. The arborization function was introduced to reproduce localized receptive fields with continuously decreasing magnitude toward their flanks. The presynaptic firing rates are drawn from a Gaussian distribution with a specific mean and covariance (see Experimental Procedures). Under the normal rearing condition, the mean firing rates ($\langle x_i \rangle$) are identical for all presynaptic neurons ($\langle x_i \rangle = 1$). The input covariance specifies that two inputs at a given retinotopic separation are more correlated if they are from the same eye compared to if they are from opposite eyes, while the correlation of two inputs with given ocular identities decreases with their retinotopic separation. MD decreases the input firing rates within the closed eye and the covariance between closed-eye and open-eye inputs by a factor $f = 0.5$ and decreases the covariance between closed-eye inputs by f^2 . To show the robustness of our learning rule to noise, we added a symmetric Gaussian random matrix (see Experimental Procedures) to the covariance matrix. While this noise heterogeneously perturbs individual synapses, it has only negligible influence on ODP.

We will use a more complex learning rule than that used previously to reproduce quantitative aspects that the simpler rule of Equations 5 and 6 could not account for. We emphasize that our point in using this more complex rule is not to argue that it captures the true, complex biological rules (see also discussion of alternatives in Supplemental Information Section S7). Rather, we only wish to demonstrate that (1) the separation of ρ and H variables gives stability despite slow homeostatic plasticity, with each form of plasticity separately zero at the network stable state and (2) suitable plasticity rules can then replicate the biological behavior without disturbing these features.

The behaviors we wish to capture with the plasticity rules are as follows (further explained in Supplemental Information Section S7). (1) TNF- α -dependent ODP: during days 3–7 of MD, there is continuing ODP toward the open eye in wild-type animals, but not in TNF- α knockouts (Kaneko et al., 2008b). Since homeostatic plasticity alone would equally scale both eyes and thus cause no ODP, this suggests that TNF- α -dependent homeostatic plasticity induces further Hebbian plasticity after Hebbian plasticity would otherwise be saturated. (2) Saturation of homeostatic plasticity: under MD in monocular cortex, homeostasis only returns synaptic strength to near its original level, which would not restore original activity levels under continuing MD. (3) Delay in homeostatic onset: no potentiation of open-eye responses is seen in binocular cortex until after day 3 of MD (Kaneko et al., 2008b). Under the simple rule of Equation 6, homeostatic plasticity, while slow, was active from the initiation of MD, yielding significant homeostatic plasticity by the time of maximal LTD (evident as the rise of $\rho_{\min}H$ by day 2 in Figure 4C).

To account for TNF- α -dependent ODP, we modified the rule for changes in the Hebbian factor by adding H dependence to ρ_{\min} :

$$\tau_{\rho} \frac{d\rho_i}{dt} = (\rho_{\max} - \rho_i)[\phi_i]_+ - (\rho_i - \rho_{\min}(H))[-\phi_i]_+. \quad (\text{Equation 7})$$

Here, $\tau_{\rho} = 0.2$ day is a characteristic time scale; ϕ_i is the pre-post covariance minus a threshold, $\phi_i = \text{Cov}[x_i, y] - \theta$ with $\theta = 0.6$, and $\rho_{\max} = 1$. We set $\rho_{\min}(H) = 0.7$ for $H \leq 1$ and $= 0.7H^{-1/2}$ for $H > 1$, which allows homeostatic plasticity to induce continued LTD and thus continued ODP after LTD has initially saturated. If ρ_{\min} is constant, there would be no ODP once LTD is saturated, while if $\rho_{\min} \sim H^{-1}$ there would be no homeostatic strengthening of depressed synapses in monocular cortex (because continued LTD would cancel homeostatic up-scaling). Apart from these constraints, the exact functional form of $\rho_{\min}(H)$ does not matter for the results.

To impose saturation of TNF- α -dependent homeostatic plasticity (Beattie et al., 2002), we first note that without saturation, homeostatic dynamics that reach the set point y_0 can be written $\tau_H dH/dt = -H + H_{\text{target}}$ with $H_{\text{target}} \equiv Hy_0/\langle y \rangle$. Here, $\langle y \rangle$ is the instantaneous (i.e., very short timescale) mean activity (used in place of y simply to average out the Gaussian input noise). To achieve saturation, we can modify the dynamics to $\tau_H dH/dt = -H + F(H_{\text{target}})$ with some saturating nonlinearity F . To impose a delay in homeostasis, we assume that, after activity decreases (e.g., due to MD), increase of the homeostatic factor H from the baseline level of 1 is delayed until a threshold

amount (which we take to be 1) of an underlying factor h has accumulated:

$$H = \text{Max}(h, 1). \quad (\text{Equation 8})$$

h is a factor that builds to a saturating value >1 when activity is below its set-point value. For example, h might be inversely related to the sensing of glutamate concentrations over time by glial cells (Stellwagen and Malenka, 2006) and would induce a proportional increase in TNF- α release once it is above a threshold. H would reflect the resulting TNF- α concentration. Note that Equation 8 incorporates the experimental result that TNF- α is only involved in upscaling strengths in response to too-low activity and not in downscaling strengths in response to too-high activity (Stellwagen and Malenka, 2006). To ensure adequate delay in homeostatic onset, h should decay to a baseline level well below 1 when this activity is at or above its set-point value. We take this baseline level to be zero. Note that these assumptions could not solve the problems of oscillations or instability in conventional models (Equations 1, 2, 3, and 4), because those models would not work with delayed homeostatic onset. In those models, the dynamics yield a fixed point that would be unstable under Hebbian plasticity alone. Therefore, for the baseline condition to be stable, they require ongoing fast homeostatic responses to return weights to the fixed point after small weight fluctuations.

Putting these assumptions together, we use the following rule (along with Equation 8) for changes in the homeostatic factor:

$$\tau_h \frac{dh}{dt} = -h + F(H_{\text{target}}). \quad (\text{Equation 9})$$

Here, $F(x)$ is a monotonically increasing function that is 0 for $x \leq 1$ (so that h returns to its baseline value of 0 once the homeostatic constraint is achieved), jumps from 0 to 1 when x exceeds 1, and then increases roughly linearly with x until it saturates at around 2 (Equation S16 and Figure S5A). We take the time constant of homeostatic plasticity to be $\tau_h = 4$ days.

We modeled MD of the contralateral eye initiated at day 0, followed by reopening of that eye at day 7, in binocular cortex. The model reproduced rapid LTD of the closed-eye synapses and slow homeostatic potentiation of the open-eye synapses (Figure 5). Hebbian LTD reduced closed-eye response by about 30% after 3 days of MD by reduction of the closed eye's Hebbian factors ρ_i (Figures 5A, 5B, and 5D). At the same time, the reduction of activity (Figure 5F) caused h to start increasing from the baseline value of 0. After about 4 days of MD, h reached the threshold value of 1, and homeostatic potentiation via increase of H was initiated (Figure 5E). The open-eye response accordingly was unchanged for the first 4 days but was potentiated by about 30% after 7 days of MD (Figures 5A and 5D). The homeostatic increase of H then started lowering the Hebbian saturation limit ρ_{\min} and decreased the closed-eye Hebbian factors, inducing additional ODP during MD days 3–7 (Figure 5C). After restoration of normal visual input at day 7, the closed-eye synapses showed rapid LTP (Figures 5A, 5B, and 5D) while homeostatic plasticity decreased back to baseline slowly (Figure 5E) so that synaptic weights overshoot their final level and then gradually decreased back to it, as we saw in the previous model of

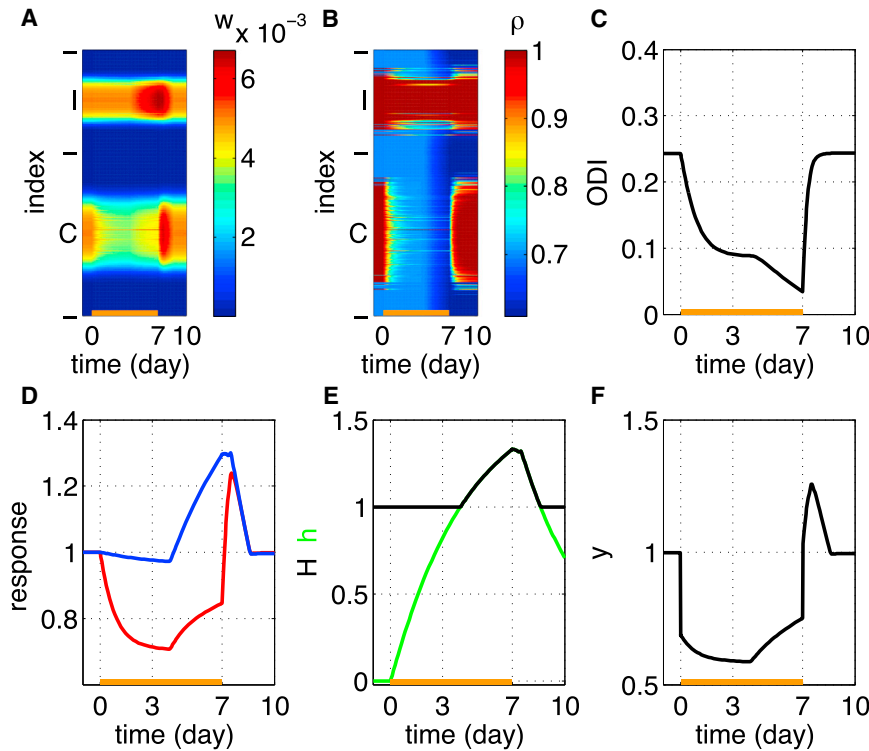


Figure 5. Simulation Results in the Binocular Cortex before, during, and after MD

MD was started at day 0, and the closed eye was reopened at day 7.

(A) Synaptic strengths w_i are shown as a function of developmental time. From bottom to top, there are 500 rows, which we label $i = 1, \dots, 500$, with the i^{th} row showing the time course of the strength of weight w_i . Indices $i = 1, \dots, 310$ are from the closed eye (contralateral eye, labeled C) and $i = 311, \dots, 500$ are from the open eye (ipsilateral eye, I). See (D) for time course of the summed weights.

(B) The Hebbian factors ρ_i .

(C) The ocular-dominance index (the value 1 means contralaterally dominated and the value -1 means ipsilaterally dominated; see [Experimental Procedures](#)).

(D) Traces of the sum of weights from the closed eye (red) and the open eye (blue), normalized to have an initial value of 1. We refer to this as the normalized visual response because it represents the relative visual response through each eye that would be assayed by an experimenter at any given time.

(E) The homeostatic factor H (black) and the underlying glial factor h (green).

(F) The average postsynaptic activity (y) during ongoing plasticity.

monocular cortex (Figure 4C). Simulation of MD in the monocular cortex using the present model (Supplemental Information Section S8) produced a result very similar to that of the single-synapse model presented in the previous section (Figure 4C).

In addition to explaining the MD results in wild-type mice, we also applied the model to ODP under various forms of inactivation (Figure 6). We modeled blockade of TrkB receptors (Kaneko et al., 2008a) as a lack of Hebbian potentiation (we removed the first LTP term from the right side of Equation 7), whether due to a direct block of LTP or to block of anatomical addition of synapses. This is based on the fact that BDNF/TrkB signaling is required for growth of synapses in neuronal cell culture (Meyer-Franke et al., 1998) and for stabilization of LTP in hippocampus (Tanaka et al., 2008; Kovalchuk et al., 2002; Figurov et al., 1996; Lai et al., 2012) and visual cortex (Sermasi et al., 2000). This reproduced the experimental results in TrkB-inactivated mice (Kaneko et al., 2008a): MD effects (both the initial LTD and the subsequent homeostatic potentiation) were normal, but the recovery from MD after reopening the closed eye was blocked (Figure 6A).

To model partial NMDA blockade during MD days 3–7, we assumed no Hebbian plasticity in the corresponding time interval (interval shaded green in Figure 6B). Purely homeostatic potentiation then equally scaled both eyes without changing ODI. The elimination of closed-eye LTD led to increased closed-eye potentiation, which in turn led to slightly less overall homeostatic upscaling than normal, slightly reducing open-eye potentiation.

To model TNF- α blockade, we assumed that H remained constant at 1 without any homeostatic adjustment. Simulations then showed little or no change in open-eye synapses over 7 days of

MD (Figure 6C), as observed in TNF- α knockout (KO) mice (Kaneko et al., 2008b). Furthermore, the model predicts that the overshoot of the previously closed-eye synapses during the recovery phase in wild-type mice (c.f., Figure 5) should be absent in TNF- α KO mice. Reopening of the previously closed eye causes that eye's Hebbian factors to be potentiated to the saturating value ρ_{\max} . In the absence of prior homeostatically induced increase in H , this simply returns those synapses to their original values without any overshoot.

Experimental Tests II: Hebbian Depression of Closed-Eye Synapses during 3–7 Days of MD and Homeostasis-Dependent Overshoot of Closed-Eye Responses during Recovery from MD

As we have noted, our proposed solution makes several robust, qualitative predictions that are independent of the model complexities that we added to more precisely match details of development. These predictions, which have not previously been tested, are as follows: (1) blockade of Hebbian plasticity during MD days 3–7 should reveal purely homeostatic plasticity, involving equal percentage increases in each eye's strengths with no change in ODI (as in Figure 6B) and (2) after MD for 7 days, long enough to yield homeostatic potentiation of synapses, restoration of normal vision should cause a TNF- α -dependent overshoot of closed-eye response above the pre-MD baseline, before it ultimately returns to the baseline (as in Figures 4C and 5D; compare Figure 6C).

We tested these predictions using intrinsic signal imaging from the binocular region of mouse V1 during MD and recovery, with results as predicted by the model (Figure 7). With intraperitoneal

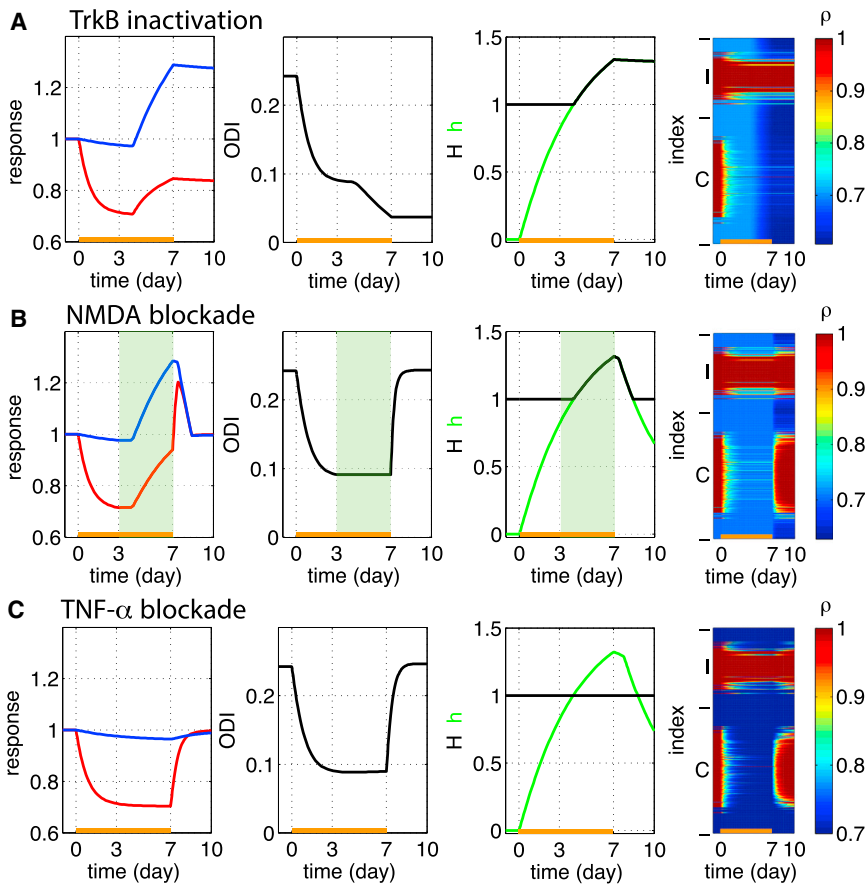


Figure 6. Results of MD, Days 0–7, and Recovery, Days 7–10, under Various Inactivation Conditions

Conventions are as in Figure 5.

(A) Simulation of TrkB-inactivated mice, modeled as an absence of LTP. MD effects (both LTD and homeostatic plasticity) were normal, but synaptic strengths did not recover under binocular vision.

(B) Simulation of partial NMDA blockade during MD days 3–7, modeled as no Hebbian plasticity during colored interval. This stopped ODP, increasing closed-eye strengthening (due to block of LTD) and slightly decreasing open-eye strengthening.

(C) Simulation of TNF- α inactivation, modeled as H remaining constant at $H=1$. No homeostatic potentiation of the open-eye synapses occurred. As a result, overshoot of synaptic strengths did not occur during the recovery period.

injections of the NMDA receptor blocker CPP during MD days 3–7, equal potentiation of the two eyes occurred without change in ODI and with increased closed-eye potentiation and reduced open-eye potentiation (Figure 7A). This is consistent with the idea (Figure 6B) that CPP blocked Hebbian LTD of the closed eye, revealing purely homeostatic plasticity, which is equal in the two eyes, while reducing the overall strength of homeostatic plasticity. Furthermore, normal recovery from MD produced the predicted overshoot of closed-eye responses followed by slow recovery to baseline, whereas if homeostatic plasticity had been blocked during MD by cortical infusion of sTNFR1 (soluble TNF receptor, which scavenges TNF- α), this overshoot did not occur (Figure 7B). Note that during normal recovery, both closed- and open-eye synapses showed a similar degree of potentiation from the pre-MD baseline at 24 hr, when the peak of the closed-eye overshoot was measured, and both recovered to near the pre-MD baseline, without further change in ODI (not shown), over the next 24 hr. This is consistent with the idea that, at 24 hr, both eyes have saturated Hebbian LTP and are scaled by the same homeostatic factor and that over the next day this homeostatic factor subsides to baseline (as in Figure 5D).

DISCUSSION

Hebbian and homeostatic plasticity work in tandem refining neural circuitry, but their interactions have been unclear. In this

paper, we have studied the dynamic interaction of fast NMDA-receptor-dependent Hebbian plasticity and slow TNF- α -mediated homeostatic plasticity as found in ocular dominance plasticity (ODP) (Kaneko et al., 2008b). While our studies were based on specific, simplified models, they revealed more general principles that we now summarize.

In most existing models, the two forms of plasticity each modify the same factor, the synaptic strength. An equilibrium is reached when the changes induced by the two are equal and opposite, meaning that homeostatic plasticity is stabilizing a set of strengths that would be unstable under Hebbian plasticity alone. We have shown that these models fail to robustly reproduce ODP because slow homeostatic negative feedback cannot stabilize fast Hebbian plasticity, which is a positive feedback process (Cooper et al., 2004; Zenke et al., 2013).

We show instead that ODP can robustly be captured by a model in which the two forms of plasticity modify separate factors whose product is the synaptic strength. Each form of plasticity then separately reaches its own stable state. This allows homeostatic plasticity to scale synaptic strengths slowly without needing to stabilize Hebbian plasticity. This model is consistent with the apparently multiplicative scaling of weights by homeostatic plasticity (Turrigiano et al., 1998; Stellwagen and Malenka, 2006; Kaneko et al., 2008b) and the independence from TNF- α levels of the percentage change in weights induced by LTP and LTD (Stellwagen and Malenka, 2006), and it has natural biophysical interpretations (Figure 4). The model can equivalently be regarded as one in which both processes directly modify the synaptic strength, but with two new features. (1) Homeostatic plasticity responds to instantaneous activity, rather than to delayed activity signals (e.g., due to slow temporal averaging), which lead to oscillations and instability. The slowness of homeostatic plasticity then results from slow learning (small weight changes per unit time) and/or delayed onset, neither of which

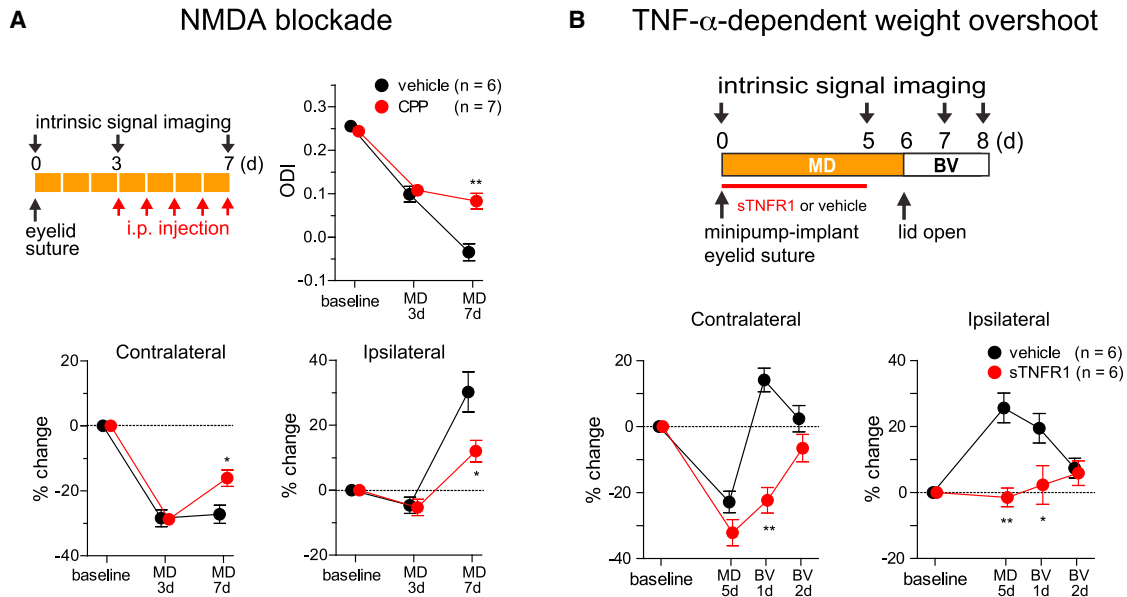


Figure 7. Experimental Verification of Model Predictions for MD and Recovery

(A) Injection of NMDA receptor antagonist CPP during days 3–7 of contralateral-eye MD reveals pure homeostatic plasticity, as judged by equal multiplicative upscaling of both eyes' responses with no further shift in ODI (upper right panel). Upper left panel indicates the experimental schedule. CPP added closed-eye potentiation and reduced open-eye potentiation (lower panels) as in Figure 6B (compare with Figure 5D). Baseline response levels were indistinguishable in CPP and control animals (Figure S7).

(B) Upon recovery from MD, there is a TNF- α -dependent overshoot (blocked by sTNFR1, which scavenges TNF- α) of the closed-eye weight from its pre-MD baseline level before it returns to baseline. MD, monocular deprivation; BV, binocular vision (to induce recovery of closed-eye responses). Bottom: change relative to day 0 baseline. * $p < 0.05$, ** $p < 0.01$, between CPP- and vehicle-injected animals in (A) between sTNFR1- and vehicle-treated animals in (B) (two-way ANOVA followed by multiple comparisons with Bonferroni correction). Data are represented as mean \pm SEM.

could stabilize fast unstable Hebbian plasticity and, thus, neither of which could be used in existing models. (2) Homeostatic plasticity also scales the minimal and maximal strengths, allowing multiplicative scaling of all strengths and allowing Hebbian plasticity, which ceases at these limiting strengths, to remain in its own stable state while homeostatic plasticity proceeds. The model can account for ODP in response to MD in both monocular and binocular cortices and under various inactivation conditions.

The model makes several predictions that we verified experimentally. First, it predicts that both forms of plasticity should be inactive at a steady state of the strengths. We tested this prediction in mouse V1, blocking Hebbian plasticity either during normal rearing or during days 7–10 of MD during the critical period for monocular deprivation. In both cases, the blockade did not alter synaptic weights, indicating that both forms of plasticity were inactive under these conditions. Second, blocking Hebbian plasticity during MD 3–7 days revealed pure homeostatic potentiation of both eyes without any ODP, including closed-eye potentiation and reduced open-eye potentiation (Figure 7A), as the model predicts (Figure 6B). Finally, we verified (Figure 7B) the predictions that during binocular recovery after 6 days of MD, the previously closed eye's synaptic strengths will overshoot their pre-MD baseline before returning to baseline (Figure 5D) and that this overshoot will not occur if TNF- α -mediated homeostasis was blocked during MD (Figure 6C). In the model, overshoot occurs because eye reopening causes rapid

potentiation of the Hebbian factor from its MD-depressed state, while the homeostatic factor only slowly decreases from its MD-elevated state.

A similar two-factor learning rule was previously independently studied in a model of the development of V1 orientation selectivity and its contrast invariance (Pool and Mato, 2010). That paper motivated the rule simply as a means of modeling multiplicative homeostatic scaling and did not address the dynamical issues we address here.

Additional Contributions to Cortical Plasticity

Many other mechanisms are likely to contribute to cortical plasticity besides the interaction of fast Hebbian and slow homeostatic plasticity studied here. For example, here we did not model plasticity in synapses to or from inhibitory neurons (e.g., Gandhi et al., 2008; Kuhlman et al., 2013; Maffei et al., 2006) or in intrinsic intracortical synapses (e.g., Trachtenberg and Stryker, 2001). We have focused on physiological ODP, ignoring mechanisms of anatomical plasticity such as branching and retraction of axons (Antonini and Stryker, 1993; Trachtenberg and Stryker, 2001). A variety of mechanisms not considered here may contribute to closing the critical period for MD-induced ODP (reviewed in Bavelier et al., 2010; Espinosa and Stryker, 2012). Cho et al. (2009) found in layer 4 that open-eye potentiation after MD is NMDA dependent. Our results partially reconcile this with the result of Kaneko et al. (2008b) that such potentiation depends on TNF- α , showing

that partial NMDA blockade reduces open-eye potentiation by eliminating closed-eye LTD and thus reducing homeostatic up-scaling. However, Hebbian LTP, laminar differences, or other facts might also play roles (further discussed in [Supplemental Information Section S7.1](#)). We have modeled only TNF- α -dependent homeostatic plasticity, which mediates scaling up of strengths in response to reduced activity, while ignoring separate mechanisms that scale synapses down in response to hyperactivity ([Stellwagen and Malenka, 2006](#)) and other forms of homeostatic plasticity ([Turrigiano, 2011](#)).

Functional Significance

The slow activation of TNF- α may mechanistically result from the diffusive signaling interactions between neurons and glia ([Stellwagen and Malenka, 2006](#)). Is there a functional reason, a computational benefit, for evolution to select this slow means of maintaining an activity set point? Consider an extreme example: if very fast homeostatic plasticity always set the post-synaptic activity to a constant set point, this would prevent coding of differing signals with differing firing rates. Similarly, for Hebbian plasticity to learn stimulus statistics that change over minutes, hours, or a day, it may be important that homeostatic plasticity not substantially change activity statistics over these timescales.

Maintaining these two processes through separable factors allows dynamic range for coding to be maintained while allowing Hebbian mechanisms to freely learn synaptic patterns without interference. It allows stable weight patterns to be maintained without constitutively active but cancelling Hebbian and homeostatic plasticities, which might be metabolically costly. Finally, as we have seen, it allows dynamic range to be maintained slowly, relative to Hebbian learning, without oscillations or instability. Thus, the dynamical interaction we propose here may describe a key biological principle underlying memory and learning in neuronal circuits.

EXPERIMENTAL PROCEDURES

Mathematical Model

The single-input models are detailed in [Results](#). For models with $N = 500$ inputs we label inputs by $i, i = 1, \dots, 500$. The eye that drives a given input is indicated by $e_i \in \{C, I\}$ (C , contralateral eye; I , ipsilateral eye). In simulations of monocular cortex, $e_i = C$ for all i . In simulations of binocular cortex, $e_i = C, i = 1 : 310$; $e_i = I, i = 311 : 500$, which reproduces the experimentally observed ODI of about 0.25 under normal vision ([Kaneko et al., 2008b](#)). Inputs are uniformly spaced on a 1D retinotopic axis, with z_i the retinotopic position of the i^{th} input ($0 \leq z_i < 1 \forall i$). In monocular cortex, $z_i = (i - 1)/500$. In binocular cortex, $z_i = (i - 1)/310$ for $i = 1 : 310$ and $z_i = (i - 311)/190$ for $i = 311 : 500$.

Input Statistics with Multiple Presynaptic Neurons

The input firing rates are assumed to be Gaussian random variables with mean $\langle x_i \rangle$ and covariance \bar{Q}_{ij} of the form:

$$\bar{Q}_{ij} = q_{e_i, e_j} \langle x_i \rangle \langle x_j \rangle \exp \left[- \frac{(z_i - z_j)^2}{2\sigma_q^2} \right]. \quad (\text{Equation 10})$$

The correlation magnitudes are $q_{C,C} = q_{I,I} = 1$, $q_{C,I} = q_{I,C} = 0.5$; $\sigma_q = 0.2$. The mean firing rates are $\langle x_i \rangle = 1$ for normal rearing and $\langle x_i \rangle = 0.5$ for contralateral inputs under MD. To demonstrate the robustness of our plasticity rule to noise and to reproduce some biological heterogeneity, we added noise to the covariance matrix, i.e., $Q_{ij} = \bar{Q}_{ij} + 2(\xi_i + \xi_j)$, where $\{\xi_i\}$ is a set of independent random

Gaussian variables with unit variance. Note that, while this noise perturbs individual synapses, it does not affect ODP.

Visual Response and Ocular Dominance Index

The visual response C or I of the contralateral or ipsilateral eye, respectively, was defined as the sum of that eye's synaptic strengths. The ocular dominance index was $ODI = (C - I)/(C + I)$.

Simulation Methods

Numerical simulations in [Figures 1, 2, 3](#), and [4](#) (except [Figure 1C](#)) used Mathematica (using NDSolve, which uses the Livermore Solver for Ordinary Differential Equations Adaptive [LSODA] approach). Other simulations used Matlab (a modified Rosenbrock formula of order 2).

In Vivo Experiments

All procedures were approved by the Institutional Animal Care and Use Committees at University of California San Francisco, in compliance with the NIH guide for the care and use of laboratory animals. C57BL/6 male mice (Charles River Laboratories) were used. Day 0 in all experiments is P25. Eyelid suture, visual stimulation, repeated optical imaging of intrinsic signals, and quantification of response amplitude and ocular dominance were performed as described ([Kaneko et al., 2008b](#)). For the partial NMDA blockade experiments, intraperitoneal injections of 3-(2-Carboxypiperazin-4-yl)propyl-1-phosphonic acid (CPP, Tocris Bioscience) (15 mg/kg) or the vehicle solution were made every 24 hr for the duration, as indicated in [Figures 3](#) and [7](#). To inhibit TNF- α signaling, recombinant soluble TNF receptor 1 (R&D Systems) at the rate of 8.57 $\mu\text{g/hr}$ or the vehicle solution was continuously infused into the cortex using an osmotic minipump (Alzet model 1002) during MD as indicated in [Figure 7](#). For details of in vivo procedures, see [Supplemental Information Section S9](#).

SUPPLEMENTAL INFORMATION

Supplemental Information includes Supplemental Information Sections S1–S9 and can be found with this article online at <http://dx.doi.org/10.1016/j.neuron.2014.09.036>.

AUTHOR CONTRIBUTIONS

T.T. and K.D.M. developed the theory and models. T.T. conducted numerical simulations in discussion with K.D.M. M.K. carried out the experiments with the help of M.P.S. T.T. and K.D.M. wrote the manuscript, which all authors revised.

ACKNOWLEDGMENTS

The authors would like to thank Yasunori Hayashi and Yukiko Goda for discussions. Supported by RIKEN Brain Science Institute (T.T.), National Institutes of Health (NIH) T32 MH089920 (M.K.), R01 EY02874 and a Sandler Family grant from the UCSF Program in Breakthrough Biomedical Research (M.P.S.), and grant NEI-EY11001 and the Gatsby Charitable Foundation (K.D.M.).

Accepted: September 24, 2014

Published: October 22, 2014

REFERENCES

- Antonini, A., and Stryker, M.P. (1993). Rapid remodeling of axonal arbors in the visual cortex. *Science* 260, 1819–1821.
- Atwood, H.L., and Karunanithi, S. (2002). Diversification of synaptic strength: presynaptic elements. *Nat. Rev. Neurosci.* 3, 497–516.
- Bavelier, D., Levi, D.M., Li, R.W., Dan, Y., and Hensch, T.K. (2010). Removing brakes on adult brain plasticity: from molecular to behavioral interventions. *J. Neurosci.* 30, 14964–14971.

- Beattie, E.C., Stellwagen, D., Morishita, W., Bresnahan, J.C., Ha, B.K., Von Zastrow, M., Beattie, M.S., and Malenka, R.C. (2002). Control of synaptic strength by glial TNF α . *Science* 295, 2282–2285.
- Bienenstock, E.L., Cooper, L.N., and Munro, P.W. (1982). Theory for the development of neuron selectivity: orientation specificity and binocular interaction in visual cortex. *J. Neurosci.* 2, 32–48.
- Cho, K.K.A., Khibnik, L., Philpot, B.D., and Bear, M.F. (2009). The ratio of NR2A/B NMDA receptor subunits determines the qualities of ocular dominance plasticity in visual cortex. *Proc. Natl. Acad. Sci. USA* 106, 5377–5382.
- Cooper, L., Intrator, N., Blais, B., and Shouval, H.Z. (2004). *Theory of cortical plasticity*. (Singapore: World Scientific).
- Espinosa, J.S., and Stryker, M.P. (2012). Development and plasticity of the primary visual cortex. *Neuron* 75, 230–249.
- Figurov, A., Pozzo-Miller, L.D., Olafsson, P., Wang, T., and Lu, B. (1996). Regulation of synaptic responses to high-frequency stimulation and LTP by neurotrophins in the hippocampus. *Nature* 381, 706–709.
- Frenkel, M.Y., and Bear, M.F. (2004). How monocular deprivation shifts ocular dominance in visual cortex of young mice. *Neuron* 44, 917–923.
- Gandhi, S.P., Yanagawa, Y., and Stryker, M.P. (2008). Delayed plasticity of inhibitory neurons in developing visual cortex. *Proc. Natl. Acad. Sci. USA* 105, 16797–16802.
- Harvey, C.D., and Svoboda, K. (2007). Locally dynamic synaptic learning rules in pyramidal neuron dendrites. *Nature* 450, 1195–1200.
- Heynen, A.J., Yoon, B.J., Liu, C.H., Chung, H.J., Hugarir, R.L., and Bear, M.F. (2003). Molecular mechanism for loss of visual cortical responsiveness following brief monocular deprivation. *Nat. Neurosci.* 6, 854–862.
- Hofer, S.B., Mrcic-Flogel, T.D., Bonhoeffer, T., and Hübener, M. (2006). Lifelong learning: ocular dominance plasticity in mouse visual cortex. *Curr. Opin. Neurobiol.* 16, 451–459.
- Hugarir, R.L., and Nicoll, R.A. (2013). AMPARs and synaptic plasticity: the last 25 years. *Neuron* 80, 704–717.
- Kaneko, M., Hanover, J.L., England, P.M., and Stryker, M.P. (2008a). TrkB kinase is required for recovery, but not loss, of cortical responses following monocular deprivation. *Nat. Neurosci.* 11, 497–504.
- Kaneko, M., Stellwagen, D., Malenka, R.C., and Stryker, M.P. (2008b). Tumor necrosis factor- α mediates one component of competitive, experience-dependent plasticity in developing visual cortex. *Neuron* 58, 673–680.
- Kaneko, M., Cheetham, C.E., Lee, Y.-S., Silva, A.J., Stryker, M.P., and Fox, K. (2010). Constitutively active H-ras accelerates multiple forms of plasticity in developing visual cortex. *Proc. Natl. Acad. Sci. USA* 107, 19026–19031.
- Kessels, H.W., and Malinow, R. (2009). Synaptic AMPA receptor plasticity and behavior. *Neuron* 61, 340–350.
- Kopec, C.D., Real, E., Kessels, H.W., and Malinow, R. (2007). GluR1 links structural and functional plasticity at excitatory synapses. *J. Neurosci.* 27, 13706–13718.
- Kovalchuk, Y., Hanse, E., Kafitz, K.W., and Konnerth, A. (2002). Postsynaptic induction of bdnf-mediated long-term potentiation. *Science* 295, 1729–1734.
- Kuhlman, S.J., Olivas, N.D., Tring, E., Ikrar, T., Xu, X., and Trachtenberg, J.T. (2013). A disinhibitory microcircuit initiates critical-period plasticity in the visual cortex. *Nature* 501, 543–546.
- Lai, K.-O.O., Wong, A.S.L., Cheung, M.-C.C., Xu, P., Liang, Z., Lok, K.-C.C., Xie, H., Palko, M.E., Yung, W.-H.H., Tessarollo, L., et al. (2012). TrkB phosphorylation by Cdk5 is required for activity-dependent structural plasticity and spatial memory. *Nat. Neurosci.* 15, 1506–1515.
- Lee, H.-K.K., Takamiya, K., Han, J.-S.S., Man, H., Kim, C.-H.H., Rumbaugh, G., Yu, S., Ding, L., He, C., Petralia, R.S., et al. (2003). Phosphorylation of the AMPA receptor GluR1 subunit is required for synaptic plasticity and retention of spatial memory. *Cell* 112, 631–643.
- Leonoudakis, D., Zhao, P., and Beattie, E.C. (2008). Rapid tumor necrosis factor α -induced exocytosis of glutamate receptor 2-lacking AMPA receptors to extrasynaptic plasma membrane potentiates excitotoxicity. *J. Neurosci.* 28, 2119–2130.
- Maffei, A., and Turrigiano, G.G. (2008). Multiple modes of network homeostasis in visual cortical layer 2/3. *J. Neurosci.* 28, 4377–4384.
- Maffei, A., Nataraj, K., Nelson, S.B., and Turrigiano, G.G. (2006). Potentiation of cortical inhibition by visual deprivation. *Nature* 443, 81–84.
- Matsuzaki, M., Honkura, N., Ellis-Davies, G.C.R., and Kasai, H. (2004). Structural basis of long-term potentiation in single dendritic spines. *Nature* 429, 761–766.
- Meyer-Franke, A., Wilkinson, G.A., Kruttgen, A., Hu, M., Munro, E., Hanson, M.G., Jr., Reichardt, L.F., and Barres, B.A. (1998). Depolarization and cAMP elevation rapidly recruit TrkB to the plasma membrane of CNS neurons. *Neuron* 21, 681–693.
- Miller, K.D., and MacKay, D.J.C. (1994). The role of constraints in Hebbian learning. *Neural Comput.* 6, 100–126.
- Miller, K.D., Keller, J.B., and Stryker, M.P. (1989). Ocular dominance column development: analysis and simulation. *Science* 245, 605–615.
- Mrcic-Flogel, T.D., Hofer, S.B., Ohki, K., Reid, R.C., Bonhoeffer, T., and Hübener, M. (2007). Homeostatic regulation of eye-specific responses in visual cortex during ocular dominance plasticity. *Neuron* 54, 961–972.
- O'Connor, D.H., Wittenberg, G.M., and Wang, S.S.-H. (2005). Graded bidirectional synaptic plasticity is composed of switch-like unitary events. *Proc. Natl. Acad. Sci. USA* 102, 9679–9684.
- Oja, E. (1982). A simplified neuron model as a principal component analyzer. *J. Math. Biol.* 15, 267–273.
- Petersen, C.C., Malenka, R.C., Nicoll, R.A., and Hopfield, J.J. (1998). All-or-none potentiation at CA3-CA1 synapses. *Proc. Natl. Acad. Sci. USA* 95, 4732–4737.
- Pool, R.R., and Mato, G. (2010). Hebbian plasticity and homeostasis in a model of hypercolumn of the visual cortex. *Neural Comput.* 22, 1837–1859.
- Sato, M., and Stryker, M.P. (2008). Distinctive features of adult ocular dominance plasticity. *J. Neurosci.* 28, 10278–10286.
- Sermasi, E., Margotti, E., Cattaneo, A., and Domenici, L. (2000). Trk B signaling controls LTP but not LTD expression in the developing rat visual cortex. *Eur. J. Neurosci.* 12, 1411–1419.
- Shepherd, J.D., and Hugarir, R.L. (2007). The cell biology of synaptic plasticity: AMPA receptor trafficking. *Annu. Rev. Cell Dev. Biol.* 23, 613–643.
- Shin, S.M., Zhang, N., Hansen, J., Gerges, N.Z., Pak, D.T.S., Sheng, M., and Lee, S.H. (2012). GKAP orchestrates activity-dependent postsynaptic protein remodeling and homeostatic scaling. *Nat. Neurosci.* 15, 1655–1666.
- Steinmetz, C.C., and Turrigiano, G.G. (2010). Tumor necrosis factor- α signaling maintains the ability of cortical synapses to express synaptic scaling. *J. Neurosci.* 30, 14685–14690.
- Stellwagen, D., and Malenka, R.C. (2006). Synaptic scaling mediated by glial TNF- α . *Nature* 440, 1054–1059.
- Sun, Q., and Turrigiano, G.G. (2011). PSD-95 and PSD-93 play critical but distinct roles in synaptic scaling up and down. *J. Neurosci.* 31, 6800–6808.
- Taha, S., and Stryker, M.P. (2002). Rapid ocular dominance plasticity requires cortical but not geniculate protein synthesis. *Neuron* 34, 425–436.
- Taha, S., Hanover, J.L., Silva, A.J., and Stryker, M.P. (2002). Autophosphorylation of alphaCaMKII is required for ocular dominance plasticity. *Neuron* 36, 483–491.
- Tanaka, J., Horiike, Y., Matsuzaki, M., Miyazaki, T., Ellis-Davies, G.C.R., and Kasai, H. (2008). Protein synthesis and neurotrophin-dependent structural plasticity of single dendritic spines. *Science* 319, 1683–1687.
- Toyoizumi, T., and Miller, K.D. (2009). Equalization of ocular dominance columns induced by an activity-dependent learning rule and the maturation of inhibition. *J. Neurosci.* 29, 6514–6525.
- Toyoizumi, T., Miyamoto, H., Yazaki-Sugiyama, Y., Atapour, N., Hensch, T.K., and Miller, K.D. (2013). A theory of the transition to critical period plasticity: inhibition selectively suppresses spontaneous activity. *Neuron* 80, 51–63.
- Trachtenberg, J.T., and Stryker, M.P. (2001). Rapid anatomical plasticity of horizontal connections in the developing visual cortex. *J. Neurosci.* 21, 3476–3482.

- Turrigiano, G.G. (2008). The self-tuning neuron: synaptic scaling of excitatory synapses. *Cell* 135, 422–435.
- Turrigiano, G. (2011). Too many cooks? Intrinsic and synaptic homeostatic mechanisms in cortical circuit refinement. *Annu. Rev. Neurosci.* 34, 89–103.
- Turrigiano, G.G., Leslie, K.R., Desai, N.S., Rutherford, L.C., and Nelson, S.B. (1998). Activity-dependent scaling of quantal amplitude in neocortical neurons. *Nature* 391, 892–896.
- von der Malsburg, C. (1973). Self-organization of orientation sensitive cells in the striate cortex. *Kybernetik* 14, 85–100.
- Yoon, B.-J., Smith, G.B., Heynen, A.J., Neve, R.L., and Bear, M.F. (2009). Essential role for a long-term depression mechanism in ocular dominance plasticity. *Proc. Natl. Acad. Sci. USA* 106, 9860–9865.
- Zenke, F., Hennequin, G., and Gerstner, W. (2013). Synaptic plasticity in neural networks needs homeostasis with a fast rate detector. *PLoS Comput. Biol.* 9, e1003330.
- Zhou, Q., Homma, K.J., and Poo, M.M. (2004). Shrinkage of dendritic spines associated with long-term depression of hippocampal synapses. *Neuron* 44, 749–757.

Neuron, Volume 84

Supplemental Information

Modeling the Dynamic Interaction of Hebbian and Homeostatic Plasticity

Taro Toyozumi, Megumi Kaneko, Michael P. Stryker, and Kenneth D. Miller

Supplemental Information

Contents

S1 BCM learning rule: Why the results of Fig. 1C are general	1
S2 Parameter choices for the model that adds stable Hebbian terms and a homeostatic term; Related to Fig. 2	3
S3 Phase-plane analysis of two models of MD in the monocular cortex; Related to Figs. 2 and 4	4
S4 Stability of the two-factor, single-synapse model of plasticity; Related to Fig. 4	6
S5 Mathematical relationship between the two factor and conventional model; Related to Figs. 2 and 4-6	9
S5.1 Single-synapse model	9
S5.2 Multi-synapse model	10
S6 Parameter dependency of the simple two factor model; Related to Fig. 4C	10
S7 Model modifications for the multi-synapse model; Related to Figs. 5 and 6	12
S7.1 Modification of the homeostatic and Hebbian rules	12
S7.2 The arbor function	14
S8 MD results of the two-factor, multi-input model in the monocular cortex; Related to Fig. 5	14
S9 Experimental Methods; Related to Figs. 3 and 7	15

S1 BCM learning rule: Why the results of Fig. 1C are general

In Fig. 1C, we showed the behavior of the BCM rule plotted against x , the value of the input activity during MD, and τ_θ/τ_w , the speed of homeostatic plasticity relative to Hebbian plasticity. Here we show that those results are general, independent of assumptions as to the values of the model parameters.

To see this, we transform the variables of the BCM learning rule (Eqs. 1-2). Let $[t]$ denote units of time. If x , y , y_0 and θ all have units of firing rate or $1/[t]$, and w is dimensionless, then for dimensional consistency Eq. 1 should take the form

$$\tau_w \frac{dw}{dt} = kxy(y - \theta) \tag{S1}$$

where k is a constant with units of $[t^3]$. In Eq. 1, we implicitly worked in units in which $k = 1$. Taking the BCM equations to be Eqs. S1 and 2, we define the dimensionless variables $\eta_x \equiv wx/y_0$, $\varphi \equiv \theta/y_0$, $\alpha_x \equiv kx^2y_0\tau_\theta/\tau_w$, and $s \equiv t/\tau_\theta$. We have indexed η_x and α_x by x because their values will change when the input activity levels x change, as under MD. In terms of these dimensionless variables we can rewrite the BCM equations as

$$\frac{d\eta_x}{ds} = \alpha_x \eta_x (\eta_x - \varphi) \quad (\text{S2})$$

$$\frac{d\varphi}{ds} = -\varphi + \eta_x^2, \quad (\text{S3})$$

whose unique fixed point is $\eta_x = \varphi = 1$. For a fixed x , the stability of the fixed point depends only on the dimensionless parameter α_x , and the behavior of the model more generally is characterized entirely by α_x and the initial values of η_x and φ at $t = 0$.

We assume that the input activity is x_0 under normal vision and is reduced by a factor of f to $x_{\text{MD}} = fx_0$, $0 < f < 1$, at the onset of MD. We take the initial condition under MD to be the normal-vision fixed point. This initial condition, $\eta_{x_0} = \varphi = 1$, becomes $\eta_{x_{\text{MD}}} = f$, $\varphi = 1$ under MD. Hence, dynamics of this rule under MD are completely characterized by f and $\alpha_{x_{\text{MD}}}$, or equivalently by f and $\alpha_{x_{\text{MD}}}/f^2 = \alpha_{x_0}$. That is, regardless of the choices of the parameters x_0 , y_0 , k , τ_θ , and τ_w , any models with the same f and α_{x_0} will show exactly the same behaviors of η_{x_0} and φ under normal rearing and of $\eta_{x_{\text{MD}}}$ and φ under MD.

In Fig. 1C, since we took $x_0 = 1$, the y -axis value $x = fx_0$ was equal to f for that model, so the y -axis can more generally taken to be f . Since we also took $k = 1$ and $y_0 = 1$ in that model, the x -axis value τ_θ/τ_w was equal to α_{x_0} for that model, so the x -axis can more generally taken to be α_{x_0} . The illustrated behaviors depend only on f and α_{x_0} and so these plots, with the axes taken to be f and α_{x_0} , are identical for any instantiation of the BCM model regardless of the specific choices of the underlying parameters that give the particular values of α_{x_0} .

In particular, Fig. 1C illustrates w_* , the value of the synaptic strength w at the first trough of synaptic weight under MD relative to its initial value at the onset of MD. From the definition $\eta_{x_{\text{MD}}} = wx_{\text{MD}}/y_0$ and the fact that f , x_0 , and y_0 are not changing as MD proceeds, we see that the value at the first trough relative to the initial value is the same for $\eta_{x_{\text{MD}}}$ as it is for w , so the plotted values of w_* vs. f and α_{x_0} are identical for any model. Fig. 1C also illustrates the stability or instability of the MD fixed point, which is determined simply by f and α_{x_0} , and measures the degree of stability by $-\text{Re } \lambda \tau_\theta$ where λ is the eigenvalue with largest real part of the BCM equations linearized about the MD fixed point. This stability measure is based on the following: if $\tilde{\lambda}$ is the corresponding eigenvalue of the dimensionless BCM equations, the amplitude of the corresponding eigenvalue develops in time as $e^{\tilde{\lambda}s} = e^{\tilde{\lambda}t/\tau_\theta} = e^{\lambda t}$ where the eigenvalue of the original equation is related to that of the dimensionless equation by $\tilde{\lambda} = \lambda \tau_\theta$. Thus, the stability index is simply $-\text{Re } \tilde{\lambda}$, which depends only on f and α_{x_0} .

The BCM rule often includes saturation of Eq. S1 at high y , rather than unlimited, quadratic-in- y growth of $\frac{dw}{dt}$. Therefore it is important to note that our conclusions would not be affected by incorporating such saturation. First, the stability of the fixed point,

$y = wx = \theta = y_0$, is determined by the local properties of Eq. S1 in the vicinity of the fixed point, whereas – to allow sufficient LTP – saturation must occur at values of y well above the fixed-point value. Thus saturation will not affect stability. Next, the value w_* of the synaptic strength at the first trough is invariant to the $y > \theta$ part of Eq. S1 because, starting from the baseline fixed point, the synapse never undergoes LTP until it reaches w_* . Taking these points together, the conclusion of Fig. 1C, that it is impossible to make the adjustment of θ in the BCM rule slow enough to allow realistic closed-eye depression yet fast enough to avoid oscillations or instability, would not be altered by incorporating saturation of Eq. S1 at high y .

S2 Parameter choices for the model that adds stable Hebbian terms and a homeostatic term; Related to Fig. 2

We choose parameters of Eqs. 3–4 to reproduce the results of MD in the monocular cortex (Kaneko et al. 2008b). We choose input activity to be $x = 1$ before MD (and $x < 1$ during MD), and set $w_{\max} = 1$. These choices are arbitrary, setting the scale for the other parameters. The minimum synaptic strength is set to $w_{\min} = 0.6$ because LTD experiments typically depress synapses by $\sim 30\%$ and, more generally, a few days of MD does not eliminate all synapses. The timescale for plasticity, $\tau_w = 0.3$ day, is chosen so that the synaptic strength reduces to about 70% of the pre-MD value within 3 days of MD in the absence of homeostatic modulation (that is, if \bar{y} is held constant). The timescale for averaging the postsynaptic activity, $\tau_{\bar{y}} = 3$ days, is chosen so that homeostatic plasticity significantly potentiates the synapse after approximately 3 days of MD. Parameters $y_0 = 0.8$ and $\theta = 0.6$ are taken from an appropriate range, within which the results do not significantly change. If $y_0 \ll 1$, then homeostatic plasticity cannot be strong enough to provide sufficient homeostatic potentiation under MD and, at the same time, weak enough to not strongly suppress synaptic strength during normal rearing, which causes synapses to undergo LTD to saturation in the normal condition and thus eliminates MD-induced LTD. If $y_0 > w_{\max}$, then Hebbian and homeostatic plasticity terms are separately zero during normal rearing, which causes a problem when binocular cortex is considered (see discussion below of “condition 1”). If θ is too small, no Hebbian depression happens under a reasonable MD condition, and if θ is too large, the synapse is strongly depressed even under the normal condition. Finally, the magnitude of homeostatic plasticity $\gamma = 0.23$ is chosen so that, after MD and LTD, homeostatic plasticity returns visual response to about 90% of the pre-MD value as in the experimental observations. Larger or smaller γ lead to larger or smaller final weight values, respectively.

While the above discussion suggests that alternative parameters cannot solve the model’s problems, we cannot fully explore the parameter space of this model. Nonetheless, we can argue that the conclusions we have reached are general and parameter-independent. These conclusions are: (1) for some ranges of input the Hebbian and system fixed points will not

coincide, meaning that the two forms of plasticity are constitutively active but opposed; (2) where this is true, NMDA blockade should reveal strong weight changes due to homeostatic plasticity; and (3) when the two fixed points are sufficiently far apart, oscillations and/or instability should be seen in the vicinity of the system fixed point. Points (2) and (3) follow from point (1).

The generality of point (1) can be seen from computing the range of input x that allows a fixed point without constitutive plasticity; for the remaining x , any fixed point will have constitutive plasticity. To compute the fixed points, we use $y = wx$ and the fact that at the fixed point $y = \bar{y}$, so that, given w at the fixed point, $\bar{y} = wx$. Fixed points without constitutive plasticity will have $w = y_0/x$ (the condition for no homeostatic plasticity). The condition for no Hebbian plasticity is then either

1. $wx^2 > \theta$ and $w \geq w_{\max}$, *i.e.* $y_0x > \theta$ and $y_0 \geq w_{\max}x$, or $\theta/y_0 < x \leq y_0/w_{\max}$.
2. $wx^2 < \theta$ and $w \leq w_{\min}$, *i.e.* $y_0x < \theta$ and $y_0 \leq w_{\min}x$, or $y_0/w_{\min} \leq x < \theta/y_0$.
3. $wx^2 = \theta$, or $y_0x = \theta$.

For values of x outside of these ranges – that is, for $x > \text{Max}(\theta/y_0, y_0/w_{\min})$, $x < \text{Min}(y_0/w_{\max}, \theta/y_0)$, or $y_0/w_{\max} < x < y_0/w_{\min}$ (the latter condition translates to $w_{\min} < w < w_{\max}$, *i.e.* it is true whenever the fixed-point w is strictly inside the Hebbian bounds) – any fixed point must have constitutive, opposed Hebbian and homeostatic plasticity, *i.e.* the system and Hebbian-only fixed points will not coincide. For example, for the parameters we used in the main text, fixed points will have constitutive plasticity for all values of x *except* $0.75 \leq x \leq 0.8$.

Furthermore, both Hebbian and homeostatic plasticity must be constitutively active at least under the normal rearing condition ($x = 1$) to reproduce ODP. If $x = 1$ satisfies condition 1 or 2, Hebbian plasticity is not active in the normal condition. The summed synaptic strength is determined by the homeostatic constraint $y = y_0$. Then, if we consider inputs from two eyes in binocular cortex, any relative strengths of the two eyes – that is, any ODI – with the given summed synaptic strength will be a fixed point so long as Hebbian plasticity remains saturated for both eyes. But this causes a problem: so long as Hebbian plasticity remains inactive, perturbations of the ODI, *e.g.* due to brief MD, will never recover but will simply persist, which is against experimental observations. In addition, if $x = 1$ satisfies condition 2, there is an additional problem. In this case, Hebbian depression is already saturated during normal rearing. Hence, MD cannot induce further Hebbian depression.

S3 Phase-plane analysis of two models of MD in the monocular cortex; Related to Figs. 2 and 4

Here we use phase-plane analysis to gain an intuition for the reasons that the single-factor model of Eqs. 3-4, which involved Hebbian and homeostatic terms competing to control

changes in w , tended to show weight oscillations. We similarly show in phase-plane analysis why the two-factor model of Eqs. 5-6 does not oscillate, an issue we examine more rigorously in the next section of the Supplemental Information, in which we analyze the stability and origin of oscillations of the model of Eqs. 3-4.

We begin with the single-factor model. The differences in stability of Figs. 2A vs. 2B can be intuitively understood from the phase plane plots of Fig. S1A,B. The arrowed lines show the direction of change in the variables (w, \bar{y}) (their time derivatives) for each given value of (w, \bar{y}) , while line colors indicate the strength of the derivatives, from strongest (blue) to weakest (red). The fixed point of the dynamics, where both derivatives are zero, is given by the intersection of the two black lines: the solid black line represents the locus of points for which $\frac{dw}{dt} = 0$ (the w nullcline), while the dashed black line represents the locus for which $\frac{d\bar{y}}{dt} = 0$ (the \bar{y} nullcline).

The generalized stability of the fixed point, by which we mean whether the fixed point is approached without significant oscillations, is largely determined by the stability of the flow in the w direction (with \bar{y} fixed) at the fixed point: for small perturbations in the w direction from the fixed point, is the w -component of the flow in the opposite direction of the perturbation, back toward the fixed point (stable flow in the w direction) or is it in the same direction of the perturbation, away from the fixed point (unstable flow in the w direction)?

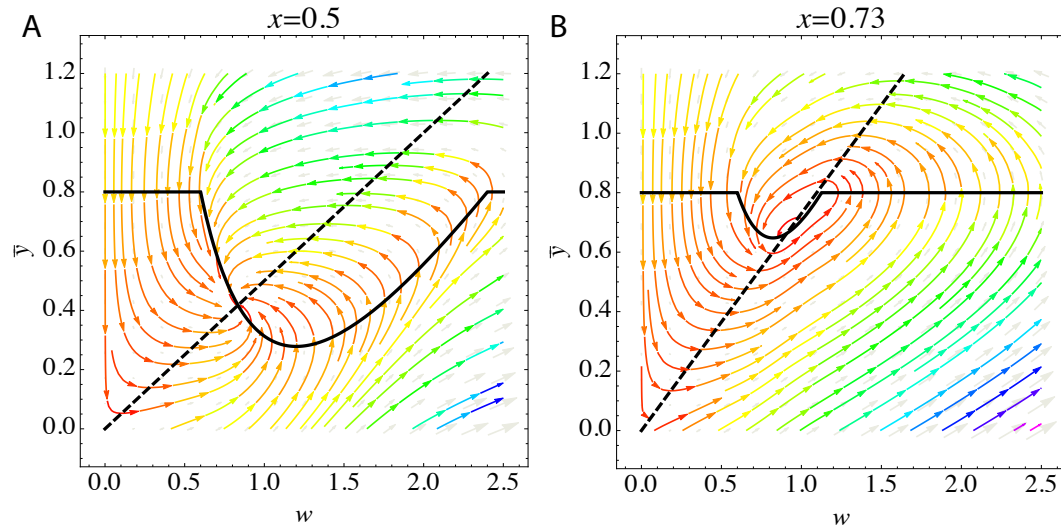


Figure S1: Phase-plane plots of Eqs. 3-4 for $x = 0.5$ (A) and $x = 0.73$ (B). The two axes specify values of averaged postsynaptic activity \bar{y} and synaptic weight w , and the lines with arrows show the direction of change in these two variables from each given point in the plane. The colors of the lines indicate the strength of the derivatives at each point, proceeding red to yellow to blue from weakest to strongest. (Strength is assayed as the length of the gradient vector $\frac{dw}{dt} \hat{\mathbf{w}} + \frac{d\bar{y}}{dt} \hat{\mathbf{y}}$ where $\hat{\mathbf{w}}$ and $\hat{\mathbf{y}}$ are unit-length vectors pointing along the w -axis and \bar{y} -axis respectively.) The solid black line shows the w -nullcline (the locus of points along which $\frac{dw}{dt} = 0$) and the dashed line shows the \bar{y} -nullcline (the locus of points along which $\frac{d\bar{y}}{dt} = 0$).

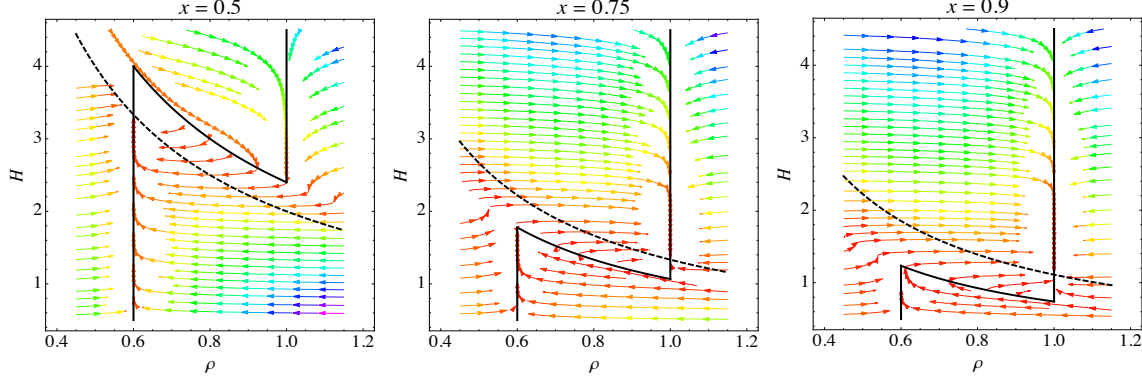


Figure S2: Phase plane analysis of the plasticity model of Eqs. 5-6. Conventions as in Fig. S1. White regions correspond to regions of very small derivatives.

If the flow is unstable in the w direction, then, because homeostatic plasticity (changes in \bar{y}) are slow relative to Hebbian changes, oscillations (or instability) will result: the perturbation will lead to large changes in w before slow changes in y lead to a reversal in the direction of changes in w (a crossing of the w nullcline), which in turn leads to a large change in w in the opposite direction as y slowly changes in the opposite direction, etc. Because the derivative $\frac{dw}{dt}$ is positive below the w nullcline and negative above the w nullcline, the flow in the w direction is unstable if the fixed point is on a positive-sloping portion of the w nullcline, as in Fig. S1B, while it is stable if the fixed point is on a negative-sloping portion of the w nullcline, as in Fig. S1A. The w nullcline transitions from negative to positive slope with increasing w . As x is increased there is a range of x for which the fixed point is found on the positive-sloping region of the w nullcline, leading to oscillations for slow homeostatic plasticity.

In contrast, phase-plane analysis of Eqs. 5-6 (Fig. S2) shows that the fixed point always occurs at one of the two limiting values of ρ , as is clear directly from Eq. 5, and that the flow in the ρ direction is always stable at these limiting values (as is also clear directly from Eq. 5).

S4 Stability of the two-factor, single-synapse model of plasticity; Related to Fig. 4

Here we analytically demonstrate the stability of the fixed point and lack of oscillations in approaching the fixed point of the two-factor, single-synapse plasticity model of Eqs. 5-6. Before more generally analyzing stability, we consider the dynamics in the limit of infinitely slow homeostasis ($\tau_H/\tau_\rho \rightarrow \infty$). For simplicity, we set $\tau_\rho = 1$ (which just sets the units of

time), so our equations are

$$\frac{d\rho}{dt} = (\rho_{max} - \rho)[xy - \theta]_+ - (\rho - \rho_{min})[\theta - xy]_+ \quad (\text{S4})$$

$$\frac{dH}{dt} = \frac{1}{\tau_H} H(1 - y/y_0) \quad (\text{S5})$$

with $w = \rho H$ and $y = wx$. Analyzing these equations for $\tau_H \rightarrow \infty$ gives an intuitive picture of why, even in the limit of extremely slow homeostasis, there are no oscillations and at most one overshoot of the synaptic weight, as shown in Fig. 5B.

Because of the assumption $\tau_H \rightarrow \infty$, we can assume that ρ always moves rapidly (relative to the slow timescale of homeostasis) to a stable fixed point of Eq. S4 for a given value of H , before H changes appreciably. For each H , these stable fixed points of ρ are given by

$$\rho(H) = \begin{cases} \rho_{max} & \text{when } H > \frac{\theta}{\rho_{max}x^2} \\ \rho_{min} & \text{when } H < \frac{\theta}{\rho_{min}x^2} \end{cases} \quad (\text{S6})$$

(Fig. S3A). Therefore, the synaptic strength converges rapidly to $\rho(H)H$ (Fig. S3B). Note that $\rho = \rho_{max}$ and $\rho = \rho_{min}$ are both stable fixed points when $\frac{\theta}{\rho_{max}x^2} < H < \frac{\theta}{\rho_{min}x^2}$, so in this case the choice between these two values of ρ depends on history. Nonetheless, there exists a unique value of H that achieves a particular synaptic strength $w = \rho(H)H$ (Fig. S3B).

The slow change in H can then be described as occurring with ρ always at its stable fixed point, so that $y = wx = \rho(H)Hx$. The dynamics of Eq. S5 can then be written

$$\frac{dH}{dt} = \frac{1}{\tau_H} H[1 - \rho(H)Hx/y_0] \quad (\text{S7})$$

Thus, H evolves so that $\rho(H)H$ approaches y_0/x ($H = 0$ is an unstable fixed point). Because there is only one value of H that achieves this, the final fixed point is unique and stable. Therefore, even when homeostatic plasticity becomes infinitely slow, there should be no oscillations of weights, but only at most one rapid transition between ρ_{max} and ρ_{min} , depending on the initial value of ρ , until synapses converge (described further in legend of Fig. S3).

Now, we analyze the stability of the fixed point of Eq. S4 for finite τ_H . Changes in τ_H do not change the locations of the fixed points, but could change their stability. However, since we saw that the fixed points are stable even for $\tau_H \rightarrow \infty$, and H provides negative feedback, it would be very surprising if reductions in τ rendered the fixed point unstable, and we will find that this does not happen.

The fixed point depends on the sign of $\phi_0 \equiv xy_0 - \theta$, and is given by: (i) $(\rho, H) = (\rho_{max}, \frac{y_0}{\rho_{max}x})$ if $\phi_0 > 0$ and (ii) $(\rho, H) = (\rho_{min}, \frac{y_0}{\rho_{min}x})$ if $\phi_0 < 0$. We will prove that the fixed point is stable and without oscillations in either case. Following standard procedures for calculating stability, we consider a small perturbation $\begin{pmatrix} \delta\rho \\ \delta H \end{pmatrix}$ from the fixed point, and consider the linearized dynamics about the fixed point:

$$\frac{d}{dt} \begin{pmatrix} \delta\rho \\ \delta H \end{pmatrix} = J \begin{pmatrix} \delta\rho \\ \delta H \end{pmatrix} \quad (\text{S8})$$

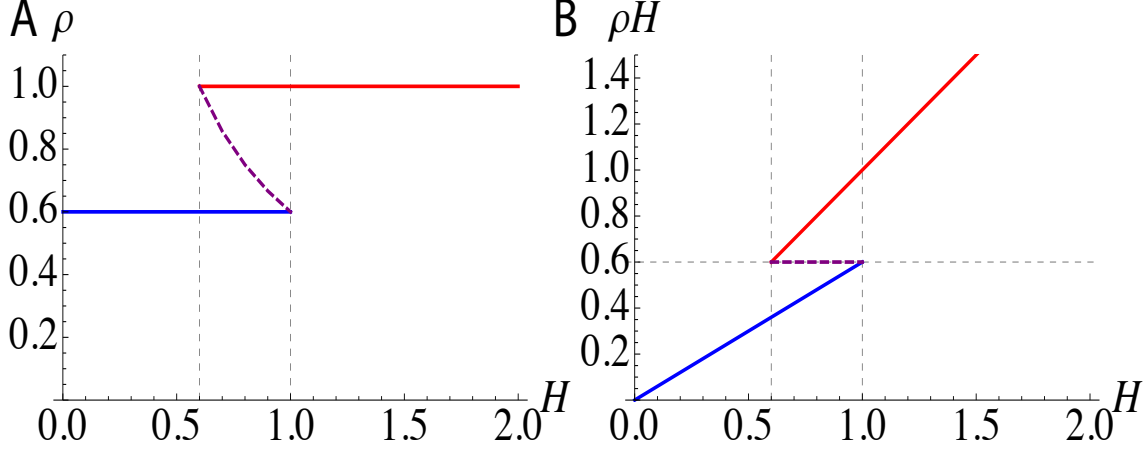


Figure S3: The two-factor model shows at most one overshoot of the synaptic weight before it converges. (A) When the homeostatic plasticity is much slower than Hebbian plasticity, the Hebbian component ρ converges rapidly for each H to its maximum value $\rho_{\max} = 1$ (red line) or minimum value $\rho_{\min} = 0.6$ (blue line). When $\frac{\theta}{\rho_{\max}x^2} < H < \frac{\theta}{\rho_{\min}x^2}$ those two values are bistable and ρ depends on its history. The dashed purple line shows the separatrix (unstable fixed points). (B) The combination of ρ and H that achieves the homeostatic constraint $wx = y_0$, *i.e.* $\rho H = y_0/x$, is unique. Under this dynamics, the synaptic weight ρH moves monotonically along whichever stable branch it starts on toward the stable fixed-point value y_0/x ; if this value can only be reached on the other branch, the weight jumps to the other branch (at constant H) when it reaches the end of the first branch, and then evolves monotonically along the second branch to the fixed point. The combination of ρ and H changes accordingly along the stable branches in (A). Thus, there is a monotonic evolution to the fixed point except for possibly one jump between the two branches.

where J is the Jacobian matrix of Eqs. S4-S5 (if r_ρ and r_H are the right-hand sides of Eqs. S4 and S5, respectively, then $J = \begin{pmatrix} \frac{\partial r_\rho}{\partial \rho} & \frac{\partial r_\rho}{\partial H} \\ \frac{\partial r_H}{\partial \rho} & \frac{\partial r_H}{\partial H} \end{pmatrix}$), evaluated at the fixed point. The stability is then determined by the eigenvalues of J . We will find that the eigenvalues are all real, indicating no oscillatory behavior around the fixed point, and negative, indicating stability.

(i) $\rho = \rho_{\max}$ and $H = \frac{y_0}{\rho_{\max}x}$ if $\phi_0 > 0$: In this case the Jacobian matrix is

$$J = \begin{pmatrix} -\phi_0 & 0 \\ -\frac{\gamma y_0}{\rho_{\max}^2 x} & -\gamma \end{pmatrix}, \quad (\text{S9})$$

and the two eigenvalues are $-\phi_0$ and $-\gamma$, which are both negative and real.

(ii) $\rho = \rho_{\min}$ and $H = \frac{y_0}{\rho_{\min}x}$ if $\phi_0 < 0$: In this case the Jacobian matrix is

$$J = \begin{pmatrix} \phi_0 & 0 \\ -\frac{\gamma y_0}{\rho_{\min}^2 x} & -\gamma \end{pmatrix}, \quad (\text{S10})$$

and the two eigenvalues are ϕ_0 and $-\gamma$, which are both negative and real. Hence, the fixed point is stable and shows no oscillatory behavior around the fixed point in either case.

S5 Mathematical relationship between the two factor and conventional model; Related to Figs. 2 and 4-6

In order to better understand this rule and to compare it to the previous rule of Eq. 3, we calculate $\frac{dw}{dt} = H \frac{d\rho}{dt} + \frac{dH}{dt} \rho$.

S5.1 Single-synapse model

We use Eqs. 5-6 to obtain the following mathematically equivalent formulation of the model:

$$\tau_\rho \frac{dw}{dt} = (H\rho_{\max} - w)[xy - \theta]_+ - (w - H\rho_{\min})[\theta - xy]_+ + \frac{\tau_\rho}{\tau_H} w \left(1 - \frac{y}{y_0}\right) \quad (\text{S11})$$

$$\tau_H \frac{dH}{dt} = H \left(1 - \frac{y}{y_0}\right) \quad (\text{S12})$$

Equation S11 has a form similar to Eq. 3 and is expressed as a sum of three terms, which correspond to the LTP, LTD, and homeostatic terms of Eq. 3 (with the homeostatic learning speed γ now explicitly represented as $\frac{\tau_\rho}{\tau_H}$). We will refer to the first two terms as the Hebbian terms and the third as the homeostatic term. Note that the factor H that scales the maximal and minimal weights is a postsynaptic-cell-specific factor that is shared across synapses if multiple synapses are considered, while the constants ρ_{\max} and ρ_{\min} might vary from synapse to synapse. The differences between Eq. S11 and Eq. 3 are:

1. The upper and lower limits of the synaptic strength, $H\rho_{\max}$ and $H\rho_{\min}$, are not fixed but are modified by homeostatic plasticity (Eq. S12).
2. The homeostatic term is driven by the instantaneous postsynaptic firing rate as opposed to the running-average of the postsynaptic firing rate in Eq. 3. Thus, there is no delay in the homeostatic term; as we have seen, delays can cause oscillations of synaptic strength.
3. A minor difference is that Eq. S11 uses linear functions $(H\rho_{\max} - w)$ and $(w - H\rho_{\min})$, whereas Eq. 3 uses threshold-linear functions $[w_{\max} - w]_+$ and $[w - w_{\min}]_+$. Thresholding would not alter the dynamics in Eq. S11 because the synaptic weight under Eqs. S11-S12 is always restricted to $H\rho_{\min} \leq w \leq H\rho_{\max}$. This may not be obvious under Eqs. S11-S12, but is obvious from the equivalent Eqs. 5-6 and the relationship $w = \rho H$.

Thus, our proposed model can equivalently be understood as one in which Hebbian and slow-but-instantaneous homeostatic plasticity both compete to modify w , but in addition homeostatic plasticity continually modifies the minimal and maximal weight values. With

homeostatic modification of limiting weight values, the Hebbian terms in Eq. S11 approach a stable state of zero plasticity with weights saturated at their limiting values, and this state remain undisturbed as homeostatic plasticity proceeds until it too reaches zero. For this reason, Eqs. S11-S12 generically reach a steady state in which there is no constitutive plasticity (*i.e.*, Hebbian and homeostatic plasticity are each separately zero), as is perhaps more obvious from the equivalent Eqs. 5-6, whereas the seemingly very similar Eq. 3 generically reaches a steady state in which Hebbian and homeostatic plasticity are each constitutively active but opposed (*i.e.* their sum is zero, but the terms individually are not zero).

S5.2 Multi-synapse model

We now use Eqs. 7-9 to compute $\frac{dw}{dt}$. We define the step function $\Theta(x)$ by $\Theta(x) = 0, x \leq 0$; $\Theta(x) = 1, x > 0$. Note that parameters ρ_{\max} and ρ_{\min} may vary across synapses though we do not make this explicit here. Then our equations become¹

$$\begin{aligned} \tau_\rho \frac{dw_i}{dt} = & (H\rho_{\max} - w_i)[\phi_i]_+ - (w_i - \sqrt{H}\rho_{\min})[-\phi_i]_+ \\ & + \Theta(H - 1) \frac{\tau_\rho}{\tau_h} w_i \left(-1 + \frac{1}{H} F\left(\frac{Hy_0}{\langle y \rangle}\right) \right) \end{aligned} \quad (\text{S13})$$

$$H = \text{Max}(h, 1) \quad (\text{S14})$$

$$\tau_h \frac{dh}{dt} = -h + F\left(\frac{Hy_0}{\langle y \rangle}\right) \quad (\text{S15})$$

Equation S13, like Eq. S11, is the sum of an LTP, an LTD, and a homeostatic term. Equation S13 is more complex than Eq. S11 for two reasons: the H -dependence of ρ_{\min} manifests as a \sqrt{H} rather than H scaling of the minimum weight (with the understanding that $H \geq 1$, Eq. S14); and the dependence of H on h manifests as the complex homeostatic plasticity term. Despite this complexity, Eq. S13 has the same three properties as we described above for Eq. S11. Thus, the multi-synapse model can again be equivalently understood as one in which Hebbian and slow-but-instantaneous homeostatic plasticity both compete to modify w , but in addition homeostatic plasticity continually modifies the minimal and maximal weight values. This again leads to a steady state in which Hebbian and homeostatic plasticity are each separately zero (no constitutive plasticity), for the same reasons just outlined for the single-synapse model.

S6 Parameter dependency of the simple two factor model; Related to Fig. 4C

In Fig. 5C, we considered relatively strong deprivation, $x = 0.5$, applied for 5 days. Here, we considered a weaker deprivation, $x = 0.75$, maintained for a long period (Fig. S4A). This led

¹We neglect the fact that the homeostatic term in Eq. S13 is also nonzero if $H = h = 1$ and $\frac{dh}{dt} > 0$. This condition holds only for an infinitesimal amount of time and hence contributes negligibly to Eq. S13.

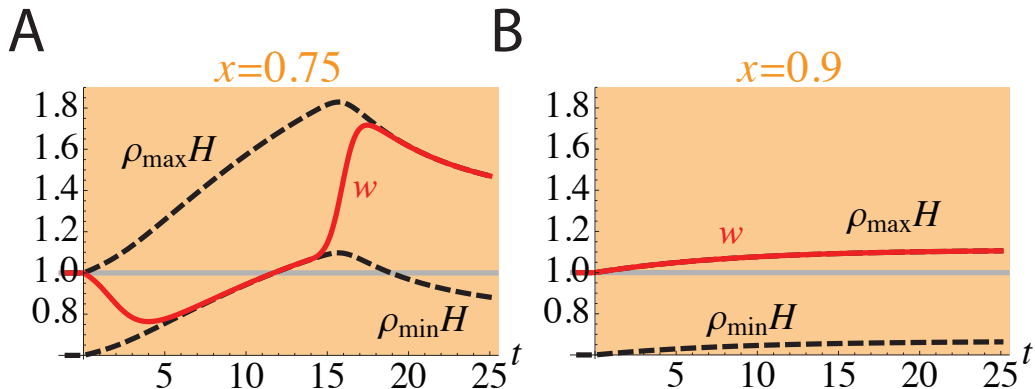


Figure S4: Simulation results of the two-factor model in the monocular cortex during mild MD. The conventions are as in Fig. 4C but input is stronger during MD. (A) For intermediate input activity during MD, the weight was depressed by Hebbian plasticity to the minimum strength, but in this case the slow homeostatic potentiation during continued MD ultimately brought the pre- and postsynaptic correlation $xy = wx^2$ above the LTP threshold θ . This induced LTP to the maximum synaptic value, followed by slow homeostatic decrease of this maximum value. (B) For large input activity during MD, there was no LTD. The synaptic strength remained at the maximal value and homeostatic plasticity slowly increased the maximal value to compensate for the slight loss of input.

to a similar trajectory of initial LTD followed by slow homeostatic scaling up of the weights. However, when we allowed the deprivation to continue for an extended period, the scaling brought the synaptic strength across the LTP/LTD threshold. At that point, just as in the case of recovery in Fig. 5C, rapid LTP increased ρ until it reached its maximal value, after which homeostatic plasticity slowly reduced the synaptic strength.

Next, we considered still weaker deprivation, $x = 0.9$ (Fig. S4B). In this case, the decrease in the input firing rate was small enough that the LTP/LTD threshold was not crossed, so there was no initial LTD and ρ remained at ρ_{\max} . Homeostatic plasticity slowly compensated for the reduction of the input by potentiating the synapse.

The strongest deprivation robustly yields the behavior we are seeking to explain: fast LTD followed by slow homeostatic compensation (Fig. 5C). For weaker deprivation, alternative behaviors are seen. The overshoot of synaptic strength after long periods of intermediate-strength deprivation (Fig. S4A) depends on homeostasis strengthening synapses sufficiently to cross the Hebbian LTD/LTP threshold, and this in turn depends on model details. It would not occur, for example, if an appropriate maximum value were imposed on H . Homeostatic strengthening in response to mild deprivation (Fig. S4B) might accurately describe the homeostatic strengthening of excitatory synapses in response to visual deprivation that occurs in layer 4 of rat visual cortex before the opening of the critical period for MD-induced ODP (Maffei et al. 2004). Before the opening of the critical period, visually-driven activity is likely to be weak relative to spontaneous activity (Toyoizumi et al. 2013), so that the

effects of deprivation on cortical activity may be relatively weak.

S7 Model modifications for the multi-synapse model; Related to Figs. 5 and 6

S7.1 Modification of the homeostatic and Hebbian rules

For the multi-synapse plasticity models, we used a more complicated homeostatic rule than the simpler rule of Eq. 6, and incorporated H -dependence of ρ_{\min} into the Hebbian rule, to try to solve several problems of the simpler rule:

- There is continued ODP towards the open eye during 3-7 days of MD that is TNF- α dependent (it does not occur in TNF- α KO animals nor in animals in which TNF- α receptors are blocked) (Kaneko et al. 2008b). To model this effect, we incorporated a reduction of ρ_{\min} with increases of the homeostatic variable H , so that increases of H allowed further LTD. The dependence on H should be weaker than a $1/H$ dependence because, otherwise, homeostatic scaling could not potentiate synapses in a depressed state.

Other factors could also contribute to TNF- α -dependent ODP, but we restricted to a single factor for simplicity. These other factors include: (1) a similar increase in ρ_{\max} with increasing H could allow TNF- α -dependent LTP of the open eye; (2) there could be a minimal, threshold level of pre-post covariance for inducing LTD, so that LTD stops at an intermediate weight level initially as LTD lowers the covariance, but resumes as TNF- α -dependent homeostatic plasticity increases the covariance; (3) Better representation of the stochasticity of neural activity and plasticity should allow a broader distribution of synaptic strengths in the normal state. Then, after 3 days of MD, a larger percentage of open-eye synapses would be in the LTD state than in our model despite an overall shift toward LTP, and similarly a larger percentage of closed-eye synapses would be in the LTP state despite a shift toward LTD. Homeostatic strengthening of response might lead Hebbian plasticity to squeeze these distributions, adding to TNF- α -dependent LTP of the open eye and LTD of the closed eye. (Note that factors like stochastic broadening of the synaptic distribution and/or a minimal covariance threshold for LTD are also necessary to explain why LTP and LTD protocols work, e.g. why in the normal state all synapses are not already saturated at the potentiated state before the protocol is applied, assuming that individual synapses are generally saturated (O'Connor et al. 2005, Petersen et al. 1998). Note also that our model fails to quantitatively account for the strength of decrease in open-eye potentiation induced by NMDA blockade. This could be fixed by factors (1) or (3) above or by further modifications of the homeostatic rule, but we neglected this for simplicity.)

- In the simple rule, homeostatic plasticity, while slow, was active from the initiation of MD. As a result, significant homeostatic plasticity had already occurred at the

time of maximal LTD (evident as the rise of $\rho_{\min}H$ by day 2 in Fig. 4C). While this caused no problem for the single-synapse model of monocular cortex studied previously, in a binocular cortex model this would mean that some potentiation of open-eye responses would already be visible at that time, unlike experiments (Kaneko et al. 2008b). This might be explained by LTD of the open eye that offsets homeostatic potentiation, but this is unlikely because no depression of open eye responses is observed in TNF- α knockout mice (Kaneko et al. 2008b). To explain this, we assumed a more complex homeostatic rule that delays the onset of homeostatic plasticity until a threshold amount of an underlying factor is accumulated. Other factors we did not consider, such as necessity of a threshold amount of activity deviation from the set point before homeostatic plasticity begins, could also or alternatively be involved.

- Stellwagen and Malenka (2006) showed that TNF- α signaling is required for scaling up of synaptic weights in response to activity blockade, but not for scaling down of synaptic weights in response to excess activity induced by inhibitory blockade. To capture this, we modified the rule so that H can increase from a baseline level of 1 (representing scaling up from baseline) but cannot decrease below 1 (meaning that scaling down from baseline is not achieved by modification of H).
- Homeostatic plasticity does not appear to perfectly compensate for activity changes. The homeostatic increase seems to be a scaling up of about 30% from the level at day 3, both in monocular and binocular cortex, which in monocular cortex restores synaptic weights to near the pre-MD level (Kaneko et al. 2008b); this would not be sufficient to restore activity to its pre-MD level under continuing MD. To match this, we made the growth of H a saturating function of the ratio of actual to set-point activity, preventing full compensation for the activity decrease. This could also be explained by a lack of activation of homeostatic plasticity by activity deviations from the set point of less than a threshold amount.

To capture these ideas, we assumed the more complex homeostatic rule of Eqs. 8–9. In Eq. 9, $F(x)$ (Eq. S16) is a monotonically increasing function that is 0 for $x \leq 1$, jumps from 0 to 1 when x exceeds 1 and then increases roughly linearly with x until it saturates at around 2. The mathematical form used was

$$F(x) = [1 + \tanh(x - 1)]\Theta(x - 1.01) \quad (\text{S16})$$

where $\Theta(z)$ is a step function, $\Theta(z) = 1$ for $z \geq 0$, $= 0$ otherwise. The shape of this function is illustrated in Fig. S5A. The argument of F is chosen to be $Hy_0/\langle y \rangle$ so that, if F did not saturate (*e.g.*, if $F(x) = x$), the stable fixed point of homeostatic plasticity, starting from a condition with $y_0/\langle y \rangle > 1$, would be $\langle y \rangle = y_0$. That is, the homeostatic rule restores the set-point activity for smaller decreases of activity, but saturation prevents full restoration for larger decreases of activity.

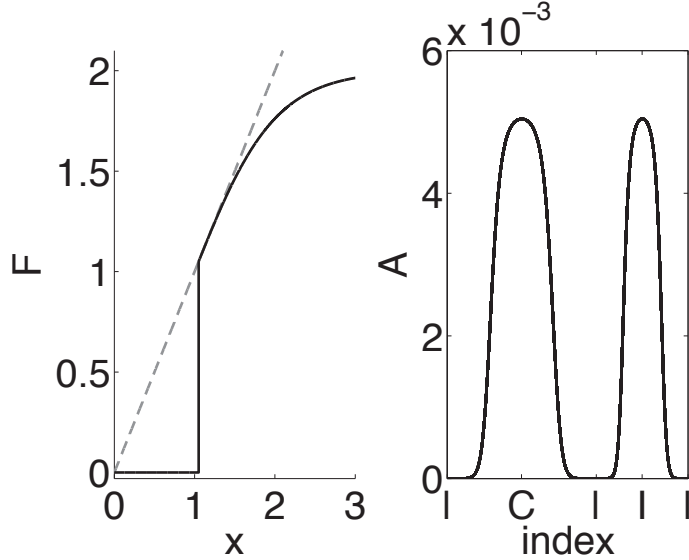


Figure S5: (A) The nonlinear function F used in Eq. 8 to update h . This function is monotonically increasing, jumping from 0 to 1 at $x \approx 1$ and then smoothly saturating at around 2. (B) The arbor function A used in the multi-synapse plasticity models for binocular cortex in the expression for synaptic strength $w_i = HA_i\rho_i$. The value of A_i (Eq. S17) is shown vs. index value i , where indices $i = 1, \dots, 310$ are from the closed eye (contralateral eye, labeled ‘C’) and $i = 311, \dots, 500$ are from the open eye (ipsilateral eye, ‘I’).

S7.2 The arbor function

The axonal arborization function A_i describes the anatomical density of axon branches to the postsynaptic neuron from a given presynaptic neuron i . The arborization strengths are given by

$$A_i \propto \frac{1}{1 + \exp(3[(z_i - 0.5)^2/(0.2)^2 - 1])}, \quad (\text{S17})$$

where the overall strengths are normalized according to $\sum_{i=1}^N A_i = 1$. The shape of this function is illustrated in Fig. S5B for the binocular case and in Fig. S6C for the monocular case.

S8 MD results of the two-factor, multi-input model in the monocular cortex; Related to Fig. 5

Here we examine the results of MD in monocular cortex for the multi-input model of Eqs. 7-9 (Fig. S6). MD to the contralateral eye was started at day 0 and the eye was re-opened at day 7. Initial LTD induced rapid decrease of the Hebbian factors, ρ , and homeostatic potentiation was induced by the delayed increase of the homeostatic factor H . Homeostatic

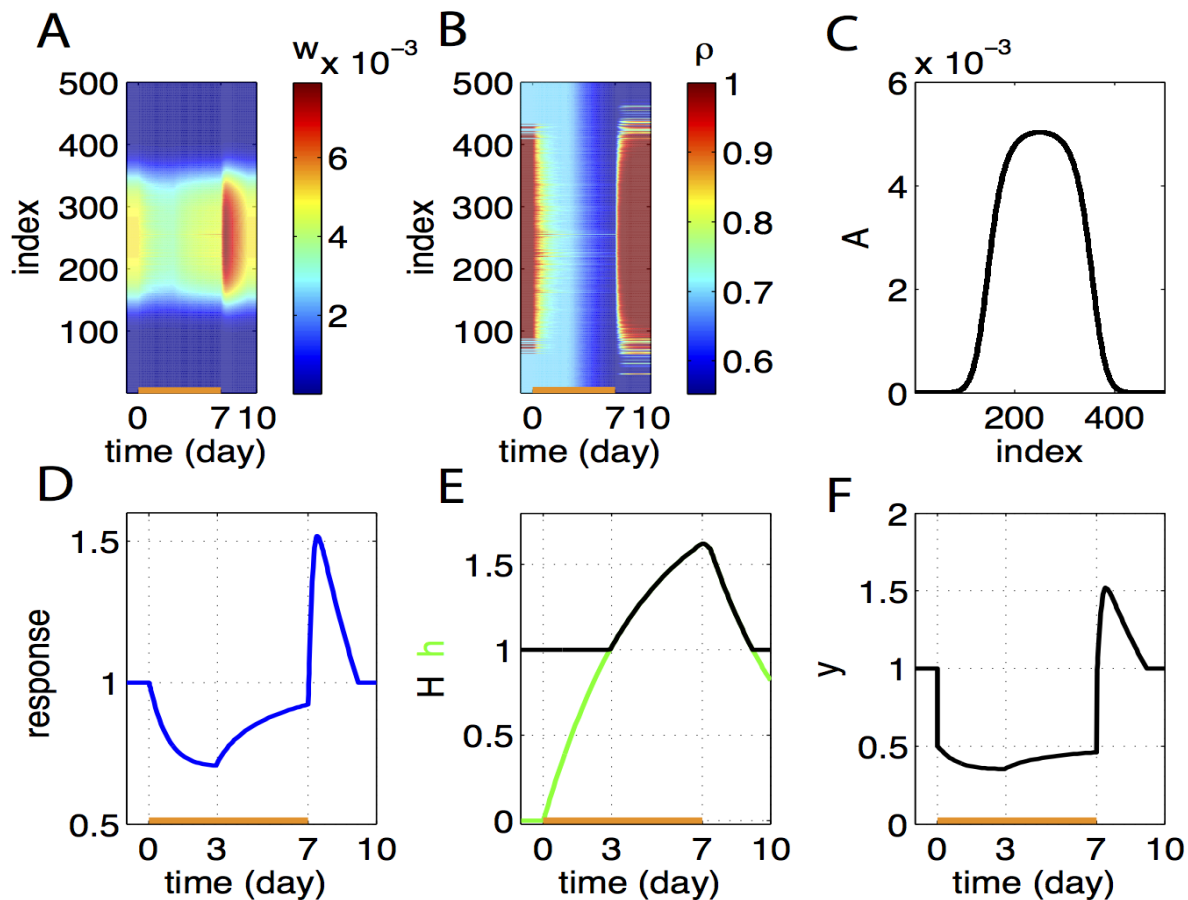


Figure S6: Simulation result in the monocular cortex before, during, and after MD using the model of Eqs. 7-9. We considered 500 inputs from the contralateral eye, which was closed during MD. MD was started at day 0 and the closed eye was re-opened at day 7. (A) Synaptic strengths w_i are shown as a function of developmental time. (B) The Hebbian factors ρ_i . (C) The arbor function A_i . (D) The normalized visual response (defined as in Fig. 5). (E) The homeostatic factor H (black) and h (green). (F) The average postsynaptic firing rate $\langle y \rangle$.

plasticity was absent for the first few days of MD because it took time for h to reach the threshold value of 1. After the re-opening of the contralateral eye, the model showed an overshoot of synaptic strengths (Fig. S6A,D), as in the single-synapse model of monocular cortex and in the multi-input model of binocular cortex. As in those cases, this behavior occurred because, after restoring normal visual input, the Hebbian component ρ potentiated rapidly and the homeostatic factor H more slowly decayed back to its baseline.

S9 Experimental Methods; Related to Figs. 3 and 7

In vivo experiments: C57BL/6 wild type breeders were purchased from Charles River Laboratories (Hollister, CA) and bred as needed. Animals were maintained in the animal

facility at University of California San Francisco and used in accordance with protocols approved by the UCSF institutional Animal Care and Use Committee. Total of 47 C57BL6 male mice were included for the analysis.

Monocular deprivation (MD) was performed by suturing shut the right eyelid (contralateral to the imaged hemisphere) at P25 as described (Kaneko et al. 2008b). The initial day of imaging was described as day 0 and other days are numbered sequentially from there. To produce recovery from effects of MD, vision was restored to the closed eye by simply removing the suture. All mice were kept under standard housing conditions with free access to food and water between recordings.

NMDA blockade: Two days prior to recording baseline responses, a custom stainless steel plate for head fixation was attached to the skull with dental acrylic under isoflurane anesthesia as described (Kaneko and Stryker, 2014). Animals were given a subcutaneous injection of carprofen (5 mg/kg) as a post-operative analgesic. The competitive NMDA receptor antagonist (R,S)-3-(2-carboxypiperazin-4-yl)propyl-1-phosphonic acid (CPP) (Tocris Bioscience) was dissolved in saline at a concentration of 1 mg/ml and the drug solution was injected intraperitoneally at a dose of 15 mg/kg roughly every 24 h, as described (Sato and Stryker 2008). The first injection in each experiment was performed right after the imaging of the corresponding day. On subsequent days, injections were made around 9AM, and imaging, if done, occurred 1-6 hours after injection (1 hr for the first mouse imaged, 6 hr for the last mouse imaged on given day). As expected, baseline response levels were indistinguishable in CPP and control animals (Fig. S7).

TNF- α blockade: Intracortical infusion of soluble TNF receptor-1 (sTNFR1, R&D Systems, Inc. Minneapolis, MN) was performed as described (Kaneko et al. 2008b, except that implantation was done on day 0). Briefly, on day 0, immediately after baseline imaging, we implanted a cortical cannula that was connected with an Alzet osmotic minipump (model 1002) filled either with vehicle solution (PBS containing 0.1% bovine serum albumin as a carrier) or 35 mg/ml of sTNFR1. This was followed immediately by eyelid suture. Infusion continued during days 0-5 of 6-day MD. On day 5, the cannula and minipump were removed and response magnitudes (MD-5d) were then recorded. On day 6, vision was restored to the closed eye by simply removing the suture to produce recovery from effects of MD, and responses were recorded 24 and 48 hours after reopening the closed eye.

Repeated optical imaging of intrinsic signals and quantification of ocular dominance were performed as described (Kaneko et al. 2008a). Briefly, during recording mice were anesthetized with 0.7% isoflurane in oxygen applied via a home-made nose mask, supplemented with a single intramuscular injection of 20-25 g chlorprothixene. Intrinsic signal images were obtained with a Dalsa 1M30 CCD camera (Dalsa, Waterloo, Canada) with a 135x50 mm tandem lens (Nikon Inc., Melville, NY) and red interference filter (610 ± 10 nm). Frames were acquired at a rate of 30 fps, temporally binned by 4 frames, and stored as 512x512 pixel images after binning the 1024x1024 camera pixels by 2x2 pixels spatially. The visual stimulus for recording in the binocular zone, presented on a 40x30 cm monitor placed 25 cm in front of the mouse, consisted of 20⁰-wide bars, which were presented between -5⁰ and 15⁰ on the stimulus monitor (0⁰ = center of the monitor aligned to center of the mouse) and moved

Figure 3B with the absolute levels of response

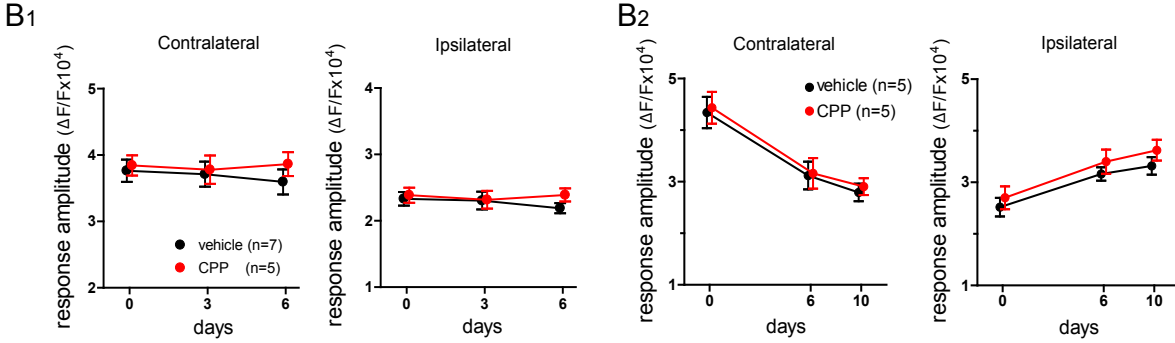


Figure 7A with the absolute levels of response

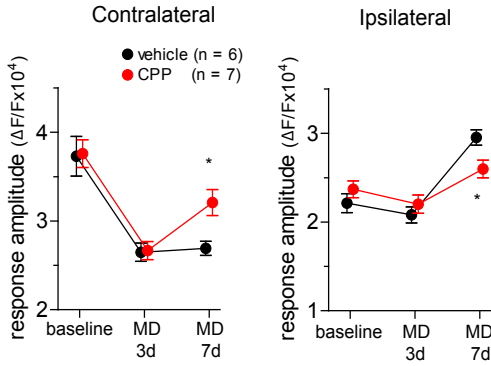


Figure S7: The CPP results in Figs. 3B and 7A remain identical when the results are shown in terms of the absolute amplitude of visual response ($\Delta F/F * 10^4$). Conventions as in Figs. 3B and 7A.

continuously and periodically upward or downward at a speed of $10^0/\text{sec}$. The phase and amplitude of cortical responses at the stimulus frequency were extracted by Fourier analysis as described (Kalatsky and Stryker, 2003). Ocular dominance index (ODI) was computed as $(R - L)/(R + L)$, where R and L are the peak response amplitudes through the right eye and the left eye, respectively, as described (Kaneko et al. 2008a). Response amplitude at each time point in individual animals was an average of at least 4 measurements.

Statistical analyses: For changes after monocular deprivation or recovery from deprivation, the response magnitude in individual animals was normalized to the baseline magnitude, followed by calculating group average and S.E.M. Response magnitudes and ocular dominance index data were analyzed by a two-way ANOVA to determine the effects of pharmacological treatments (CPP or sTNFR1) and of manipulations of visual experiences (ND, MD, or binocular recovery) in Prism 6 (GraphPad Software, CA). For multiple comparisons, Bonferroni corrections were used.

Supplemental References:

Kaneko, M., and Stryker, M.P. (2014) Sensory experience during locomotion promotes recovery of function in adult visual cortex. *eLife*, e02798.

Maffei, A., Nelson, S. B., and Turrigiano, G. G. (2004) Selective reconfiguration of layer 4 visual cortical circuitry by visual deprivation. *Nature Neurosci.*, 7(12):1353-1359.

Sato, M., and Stryker, M.P. (2008). Distinctive features of adult ocular dominance plasticity. *J. Neurosci.* 28, 7520-7536.

Kalatsky, V.A., and Stryker, M.P. (2003) New paradigm for optical imaging: temporally encoded maps of intrinsic signal. *Neuron* 38, 529-545.